

## Luminescent Mercury Complexes

## Topological Evolution in Mercury(II) Schiff Base Complexes Tuned through Alkyl Substitution – Synthesis, Solid-State Structures, and Aggregation-Induced Emission Properties

Yu-Wei Dong,<sup>[a]</sup> Rui-Qing Fan,<sup>\*[a]</sup> Xin-Ming Wang,<sup>[a]</sup> Ping Wang,<sup>[a]</sup> Hui-Jie Zhang,<sup>[a]</sup> Li-Guo Wei,<sup>[a]</sup> Yang Song,<sup>[a]</sup> Xi Du,<sup>[a]</sup> Wei Chen,<sup>[a]</sup> and Yu-Lin Yang<sup>\*[a]</sup>

**Abstract:** From two series of Schiff base ligands, (*E*)-*N*-(pyridine-2-yl)(CMe=NPhR) and (*E*)-*N*-(pyridine-2-yl)(CH=NPhR) [R = H, **L1a**, **L1b**; 2-CH<sub>3</sub>, **L2a**, **L2b**; 4-CH<sub>3</sub>, **L3a**, **L3b**; 2,6-(CH<sub>3</sub>)<sub>2</sub>, **L4a**, **L4b**; 2,6-(C<sub>2</sub>H<sub>5</sub>)<sub>2</sub>, **L5a**, **L5b**; 2,6-(*i*-C<sub>3</sub>H<sub>7</sub>)<sub>2</sub>, **L6a**, **L6b**; 2,4,6-(CH<sub>3</sub>)<sub>3</sub>, **L7a**, **L7b**], fourteen mercury(II) complexes, namely, Hg**1a**–Hg**7a** and Hg**1b**–Hg**7b** were synthesized. Their structures were established by single-crystal X-ray diffraction, and they were physically characterized by <sup>1</sup>H and <sup>13</sup>C NMR spectroscopy, ESI-MS, FTIR spectroscopy, elemental analysis (EA), and powder XRD

(PXRD). The crystal structures indicate that the position and type of substituent can directly influence the formation of 1D → 3D supramolecular metal–organic frameworks through C–H...Cl and π–π interactions. Complexes Hg**1a**–Hg**7a** and Hg**1b**–Hg**7b** display deep blue emissions at λ = 401–428 nm in acetonitrile solution and light blue emissions at λ = 443–494 nm in the solid state. It is worth noting that Hg**1a**, Hg**3a**, Hg**1b**, and Hg**3b** exhibit good aggregation-induced emission (AIE) properties in CH<sub>3</sub>CN/H<sub>2</sub>O solutions.

## Introduction

Supramolecular metal–organic frameworks (SMOFs)<sup>[1]</sup> have attracted enormous attention because of their intriguing structures and wide potential applications in different areas such as nonlinear optics, magnetism, photoluminescence, and electrochemistry.<sup>[2]</sup> SMOFs are the result of complementary interactions between two or more components in a desired thermodynamically favorable fashion through noncovalent interactions. The type of noncovalent supramolecular interaction, such as π–π stacking,<sup>[3]</sup> hydrogen bonding,<sup>[4]</sup> or secondary bonding interactions (SBIs),<sup>[5]</sup> depends on the shape and functional groups of the components that form the SMOF. Notably, appropriate hydrogen-bonding and π–π stacking interactions can produce the aggregation-induced emission (AIE) phenomenon, which was first reported by Tang et al. in 2001.<sup>[6]</sup> Therefore, the real-world applications of solid-state materials can be expanded significantly if they exhibit aggregation-induced emission. These functional materials are generally constructed from metal ions and bridging organic ligands.<sup>[7]</sup> The ligand not only provides capability for selective metal-ion coordination but also generates the desired noncovalent intermolecular interactions to di-

rect crystal packing.<sup>[8]</sup> Hence, the major challenge in supramolecular chemistry is the design and synthesis of organic ligands. After almost a century since their discovery, Schiff base ligands still play an important role in metal coordination chemistry, owing to their facile synthesis, remarkable versatility, and good solubility in common solvents.<sup>[9]</sup> In general, compared with rigid ligands, a metal-coordinated Schiff base ligand can more readily form intermolecular π...π or C–H...π interactions in the aggregated or crystal state because of the high flexibility of the imine unit.

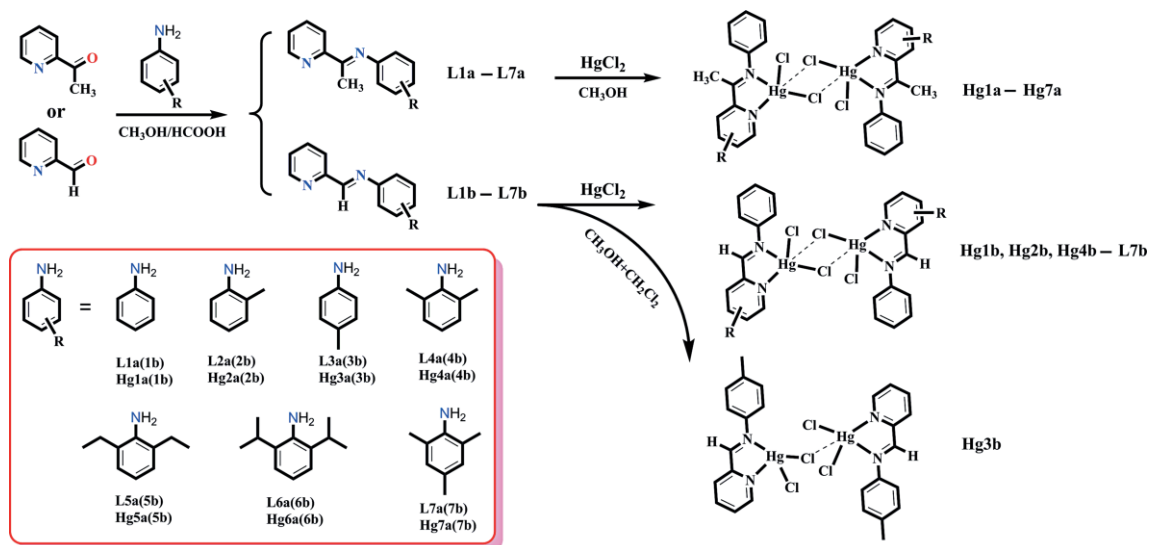
Owing to their applications in the paper industry, cosmetics, paints, fluorescent lamps, sensors, and mercury batteries,<sup>[10]</sup> mercury and its complexes are of immense importance in chemistry and related disciplines. The spherical d<sup>10</sup> configuration of the mercury(II) ion is associated with a flexible coordination environment. Furthermore, owing to the lability of d<sup>10</sup> metal complexes, the formation of coordination bonds is reversible, and the metal ions and ligands can rearrange during the supramolecular assembly to allow the formation of thermodynamically more stable structures through the variation of the coordination polyhedron and coordination number of the mercury atom.<sup>[11]</sup>

Inspired by the above discussion, herein, two series of Schiff base ligands, (*E*)-*N*-(pyridine-2-yl)(CMe=NPhR) and (*E*)-*N*-(pyridine-2-yl)(CH=NPhR), which carry different alkyl substituents on the phenyl rings (**L1a**–**L7a** and **L1b**–**L7b**, Scheme 1), have been employed for the synthesis of mercury(II) complexes. Fourteen mercury(II) complexes, namely, Hg**1a**–Hg**7a** and Hg**1b**–Hg**7b**, were prepared through the reactions of the corresponding ligands and HgCl<sub>2</sub> in 1:1 molar ratios. Subsequently, the structures of the ligands and mercury(II) complexes were

[a] MIIT Key Laboratory of Critical Materials Technology for New Energy Conversion and Storage, School of Chemistry and Chemical Engineering, Harbin Institute of Technology, 92, Xidazhi Street Nangang District, Harbin, 150001, P. R. China  
E-mail: fanruiqing@hit.edu.cn  
ylyang@hit.edu.cn

<http://homepage.hit.edu.cn/pages/fanruiqing>  
<http://homepage.hit.edu.cn/pages/yanqyulin>

Supporting information for this article is available on the WWW under <http://dx.doi.org/10.1002/ejic.201600231>.



Scheme 1. Chemical structures and synthetic routes for Schiff base ligands (**L1a-L7a** and **L1b-L7b**) and mercury(II) complexes (**Hg1a-Hg7a**, **Hg1b-Hg7b**).

characterized through <sup>1</sup>H and <sup>13</sup>C NMR spectroscopy, ESI-MS, IR spectroscopy, elemental analysis (EA), and powder XRD (PXRD); ligands **L3b** and **L6b** and complexes **Hg1a-Hg7a** and **Hg1b-Hg7b** were additionally characterized by single-crystal X-ray crystallography. Although the structure of **Hg1b** has been reported by others recently, it is included herein for comprehensive comparison.<sup>[12]</sup> In this study, we investigated the effect of related alkyl-substituted Schiff base ligands and intermolecular interactions (Hg...Cl secondary interactions, C-H...Cl hydrogen bonds, and π-π interactions) on the organization and stabilization of SMOFs. Moreover, the influence of the substituent on the photoluminescence of the compounds in CH<sub>3</sub>CN solution and in the solid state are discussed. Complexes **Hg1a**, **Hg3a**, **Hg1b**, and **Hg3b** exhibit AIE in CH<sub>3</sub>CN/H<sub>2</sub>O solutions.

## Results and Discussion

### Synthesis and Spectral Characterization

The fourteen imine ligands were prepared readily in one-step procedures through the condensation of the pyridine aldehyde derivative with the corresponding monamine in a 1:1 molar ratio in anhydrous methanol/formic acid solution. Two pyridine derivatives (2-acetylpyridine and 2-pyridinecarbaldehyde) and seven different substituted anilines were investigated (see Scheme 1). The recrystallization of **L3b** and **L6b** from *n*-hexane provided yellow crystals suitable for X-ray analysis. The yields of the fourteen imine ligands varied from 70 to 92 %. The complexes (**Hg1a-Hg7a** and **Hg1b-Hg7b**) were prepared through the reactions of HgCl<sub>2</sub> and the corresponding imine ligands in methanol or methanol/dichloromethane under reflux and obtained as good-quality crystals in good yields. All of the complexes in the solid state are stable upon extended exposure to air. The complexes are soluble in common organic solvents, such as chloroform, dimethyl sulfoxide, and acetonitrile.

The infrared spectra of **Hg1a-Hg7a** and **Hg1b-Hg7b** (see Figures S1 and S2 in the Supporting Information) are similar to

those of the corresponding ligands, and selected diagnostic bands are listed in the Exp. Section. In the IR spectra of ligands **L1a-L7a** and **L1b-L7b**, the existence of C=N bonds is demonstrated clearly by the presence of strong characteristic C=N bands in the range  $\tilde{\nu} = 1625\text{--}1669\text{ cm}^{-1}$ . The negative shifts of these bands by 2–36 cm<sup>-1</sup> in the spectra of the complexes may be attributed to the coordination of the nitrogen atom of the imine moiety to the metal ion.<sup>[13]</sup> This is further confirmed by the presence of  $\nu(\text{M-N})$  vibrations in the region  $\tilde{\nu} = 422\text{--}459\text{ cm}^{-1}$  in the spectra of all of the complexes.<sup>[14]</sup>

The <sup>1</sup>H NMR spectra of the imine ligands **L1a-L7a** and **L1b-L7b** as well as those of their mercury(II) complexes in CDCl<sub>3</sub> were recorded at room temperature (Figures S3 and S4). In the <sup>1</sup>H NMR spectra of the complexes, the chemical shifts are slightly different from those observed for the non-coordinated ligands. Of particular note are the Py-*H*<sup>6</sup> resonances of **Hg1a-Hg7a** and **Hg1b-Hg7b**, which are shifted downfield owing to the coordination of the pyridine nitrogen atom to the mercury(II) center. In the spectra of **Hg1b-Hg7b**, the resonance of the imine proton is shifted downfield by at least 0.05 ppm.<sup>[15]</sup> The position of the HC=N resonance is influenced by the alkyl groups on the adjacent phenyl ring (Figure 1). For ligands **L2b** and **L4b-L7b** in which the ring is substituted by one to three methyl groups, 2,6-(C<sub>2</sub>H<sub>5</sub>)<sub>2</sub>, or 2,6-(iC<sub>3</sub>H<sub>7</sub>)<sub>2</sub>, the peak is generally shifted upfield relative to that of **L1b**. Similarly, this peak is shifted downfield for **L3b** with a 4-CH<sub>3</sub> substituent on the phenyl ring. This is most likely caused by the better electron-donating ability and coplanarity in ligand **L3b**.

In the <sup>13</sup>C NMR spectra (Figures S5 and S6), the signals of the C=N nuclei are observed at  $\delta = 159.63\text{--}167.48\text{ ppm}$ . The ESI-MS spectra (Figures S7 and S8) each exhibit an intense peak at  $m/z = 183.09\text{--}552.74$ , which is assigned to  $[\text{M} + \text{H}]^+$ . The detailed data are listed in the Exp. Section. We performed powder X-ray diffraction for **Hg1a-Hg7a** and **Hg1b-Hg7b** to check the purity of the bulk products. In Figure S9, we can see that all major peak positions of the measured patterns are in good agreement with those simulated. Furthermore, the differences

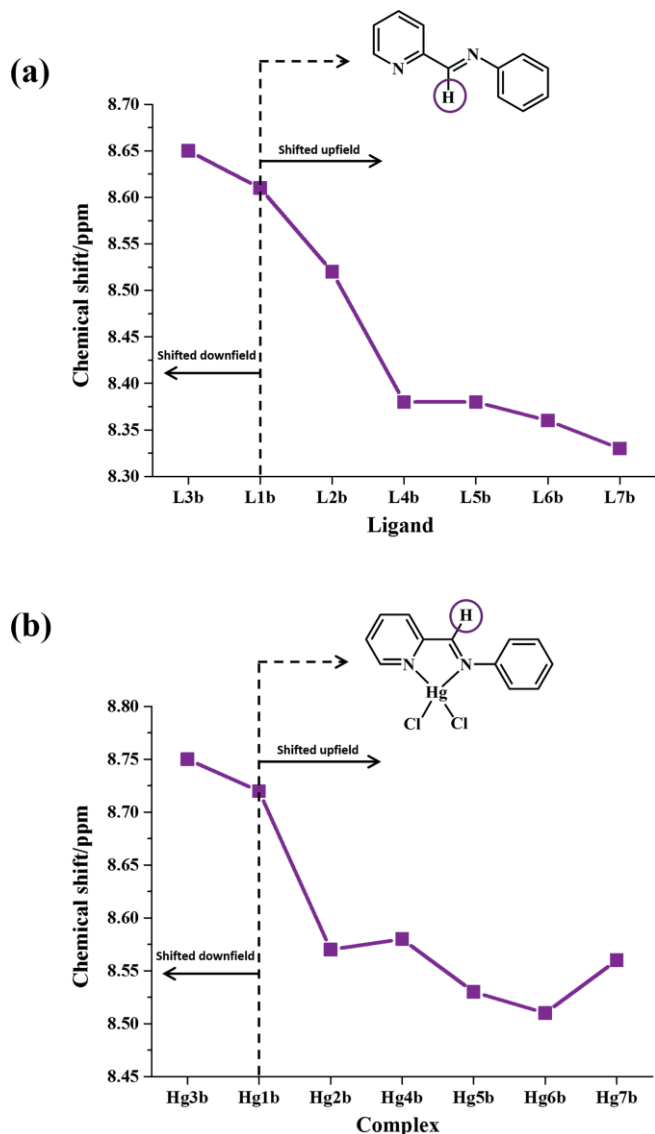


Figure 1. Change in chemical shift for the imine proton for (a) **L1b–L7b** and (b) **Hg1b–Hg7b**.

in intensity may be due to the preferred orientation of the crystal products. These observations are consistent with the crystal structures (see below). To further understand the structures of

these complexes, single crystals were obtained and analyzed by single-crystal X-ray diffraction.

## Descriptions of the Structures

### Structural Analysis of **Hg1a–Hg7a**

The coordination abilities of **L1a–L7a** were examined with mercury dichloride. The crystallographic and structural determination data for complexes **Hg1a–Hg7a** are listed in Table S1. Selected bond lengths and angles are summarized in Tables S2 and S3. The single-crystal X-ray diffraction analysis revealed that complexes **Hg1a–Hg7a** have analogous structure units, as shown in Figures 2 (a) and S10. In **Hg1a–Hg7a**, each asymmetric unit consists of one crystallographically independent  $\text{Hg}^{2+}$  ion, one coordinated Schiff base ligand **L1a–L7a**, and two chloride ions. As the van der Waals radii of Hg and Cl are 1.70 and 1.80 Å,<sup>[16]</sup> respectively, any  $\text{Hg}\cdots\text{Cl}$  distance less than 3.50 Å and any  $\text{Hg}\cdots\text{Hg}$  distance less than 3.4 Å may be considered potentially significant. Therefore, we presume that **Hg1a–Hg7a** form dimeric molecules through secondary  $\text{Hg}\cdots\text{Cl}$  interactions (the  $\text{Hg}\cdots\text{Cl}$  distances are in the range 2.864–3.260 Å, Table 1); no efficient  $d^{10}\cdots d^{10}$  weak interactions were observed (the  $\text{Hg}\cdots\text{Hg}$  distances are in the range 3.837–4.133 Å, Table 1). If the secondary  $\text{Hg}\cdots\text{Cl}$  interactions are included in the coordination spheres of the mercury(II) ions, the five-coordinate geometry indices,  $\tau_5$ , as defined by Addison and Reedijk,<sup>[17]</sup> are 0.020–0.475 for **Hg1a–Hg7a**; therefore, the coordination geometries are best described as pseudo-square-pyramidal (SQP).<sup>[18]</sup> In **Hg1a–Hg7a**, the pyridyl and phenyl rings of the corresponding ligands **L1a–L7a** are severely twisted, and the dihedral angles are close to 90° (72.279–89.145°, Table 1).

For **Hg1a**, secondary  $\text{Hg}\cdots\text{Cl}$  interactions with a distance of 2.888 Å and C–H $\cdots$ Cl (the H3A $\cdots$ Cl1 and H5A $\cdots$ Cl1 distances are 2.901 and 2.735 Å, respectively) hydrogen-bond interactions<sup>[19]</sup> link the adjacent molecules to form 1D chains. These 1D chains are further assembled into a 3D supramolecular network through  $\pi$ – $\pi$  stacking interactions (the centroid–centroid distances are 3.464 and 3.831 Å), as shown in Figure S11a. However, the mononuclear molecules of **Hg3a** are assembled into a 2D supramolecular layer through intermolecular H3A $\cdots$ Cl2, H4A $\cdots$ Cl1, and H5A $\cdots$ Cl2 hydrogen bonds (see Table S4) as well as secondary  $\text{Hg}\cdots\text{Cl}$  interactions. Moreover, interlayer  $\pi$ – $\pi$

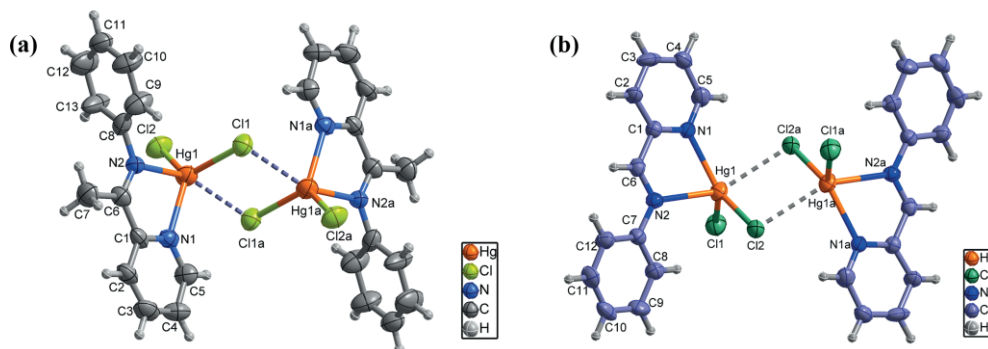


Figure 2. Molecular structures of (a) **Hg1a** and (b) **Hg1b** showing 50 % probability ellipsoids and the crystallographic numbering scheme.

Table 1. Structural and geometrical parameters for Hg1a–Hg7a and Hg1b–Hg7b.

| Complex | Coordination geometry       | Addison parameter ( $\tau$ ) | Hg...Cl bond length [Å] | Hg...Hg bond length [Å] | Dihedral angle [°] <sup>[a]</sup> | Dimensionality |
|---------|-----------------------------|------------------------------|-------------------------|-------------------------|-----------------------------------|----------------|
| Hg1a    | pseudo-square-pyramidal     | 0.475                        | 2.888(3)                | 3.936(4)                | 78.786                            | 3D             |
| Hg2a    | pseudo-square-pyramidal     | 0.020                        | 3.032(2)                | 3.837(3)                | 77.250                            | 2D             |
| Hg3a    | pseudo-square-pyramidal     | 0.462                        | 3.032(7)                | 4.042(1)                | 72.279                            | 3D             |
| Hg4a    | pseudo-square-pyramidal     | 0.370                        | 2.997(6)                | 4.101(9)                | 78.034                            | 2D             |
| Hg5a    | pseudo-square-pyramidal     | 0.099                        | 2.864(1)                | 3.860(1)                | 89.145                            | 2D             |
| Hg6a    | pseudo-square-pyramidal     | 0.117                        | 3.070(1)                | 4.133(2)                | 83.512                            | 2D             |
| Hg7a    | pseudo-square-pyramidal     | 0.420                        | 3.260(1)                | 4.103(1)                | 80.044                            | 1D             |
|         | pseudo-square-pyramidal     | 0.401                        | 3.146(1)                | 4.048(2)                | 78.999                            | –              |
| Hg1b    | pseudo-square-pyramidal     | 0.291                        | 2.881(1)                | 4.066(2)                | 11.760                            | 3D             |
| Hg2b    | pseudo-square-pyramidal     | 0.017                        | 3.098(8)                | 4.178(1)                | 47.736                            | 1D             |
| Hg3b    | trigonal pyramidal          | 0.751                        | 3.559(7)                | 4.636(1)                | 7.152                             | 3D             |
|         | pseudo-square-pyramidal     | 0.263                        | 3.458(7)                | –                       | 7.860                             | –              |
| Hg4b    | pseudo-square-pyramidal     | 0.198                        | 3.064(4)                | 4.065(9)                | 75.501                            | 1D             |
| Hg5b    | pseudo-square-pyramidal     | 0.220                        | 3.199(5)                | 4.202(9)                | 69.377                            | 1D             |
| Hg6b    | pseudo-square-pyramidal     | 0.064                        | 3.018(6)                | 4.052(9)                | 88.005                            | 1D             |
| Hg7b    | pseudo-trigonal-bipyramidal | 0.508                        | 3.078(5)                | 4.042(7)                | 83.483                            | 1D             |

[a] Between the pyridyl ring and phenyl ring.

stacking interactions with centroid–centroid distances of 3.690 Å between the two pyridine rings link the adjacent coordination layers to form a 3D network (Figure S11b). In this case, if the secondary Hg...Cl, C–H...Cl hydrogen-bond, and  $\pi$ – $\pi$  interactions are regarded as the linkers, and each mononuclear unit is viewed as the node,<sup>[20]</sup> the simplified topological representations of Hg1a and Hg3a can be described as 3D diamond-like architectures with point symbol 6<sup>5</sup>, as shown in Figures S11c and S11d, respectively.

In contrast to Hg1a and Hg3a, owing to the bigger steric hindrance of the 2-CH<sub>3</sub>, 2,6-(CH<sub>3</sub>)<sub>2</sub>, 2,6-(C<sub>2</sub>H<sub>5</sub>)<sub>2</sub>, and 2,6-(*i*-C<sub>3</sub>H<sub>7</sub>)<sub>2</sub> substituents of the phenyl rings, the mononuclear molecules of Hg2a and Hg4a–Hg6a are assembled into different 2D bilayers (Figure 3) through noncovalent interactions (i.e., C–H...Cl hydrogen bonds and  $\pi$ – $\pi$  stacking) and secondary Hg...Cl interactions only, and the 2D topological views are shown in Figure S12. Complex Hg7a displays two dimers (enantiomeric forms I and II, see Figure 4, parts a and b) of identical composition in the crystal but with different behaviors. Each type is composed of centrosymmetric [Hg(L7a)Cl<sub>2</sub>]<sub>2</sub> dimers, which are linked by a Hg–Cl<sub>2</sub>–Hg bridge. The lengths and angles of the

coordination bonds of the central ions (see Table S3) have small differences. In Hg7a, the mercury(II) ions are pseudo-five-coordinate with distorted square-pyramidal coordination geometry and the trigonality indices  $\tau = 0.420$  (Hg1) and 0.401 (Hg2). The dihedral angles between the pyridyl rings and the phenyl rings in molecules I and II are 80.044 and 78.999°, respectively (Table 1). Meanwhile, the steric arrangements in the crystal are slightly different (Figure 4, c and d). In molecule I, long-distance interactions exist between each metal center and the chloride ions of a neighboring [Hg(L7a)Cl<sub>2</sub>]<sub>2</sub> unit, and the corresponding Hg1...Cl2a (1 – x, 1 – y, 1 – z) distance is 3.260 Å, which is close to the sum of the van der Waals radii of Hg and Cl (3.50 Å); however, the Hg1...Hg1a distance of 4.103 Å yields inefficient M...M interactions.<sup>[21]</sup> However, in molecule II, the Hg2...Cl4a distance of 3.146 Å and the Hg2...Hg2a distance of 4.048 Å indicate that the interactions between the [Hg(L7a)Cl<sub>2</sub>]<sub>2</sub> units are slightly stronger than those in I. The dimers of I and II are assembled through intermolecular C2–H2a...Cl2 (2.712 Å), C5–

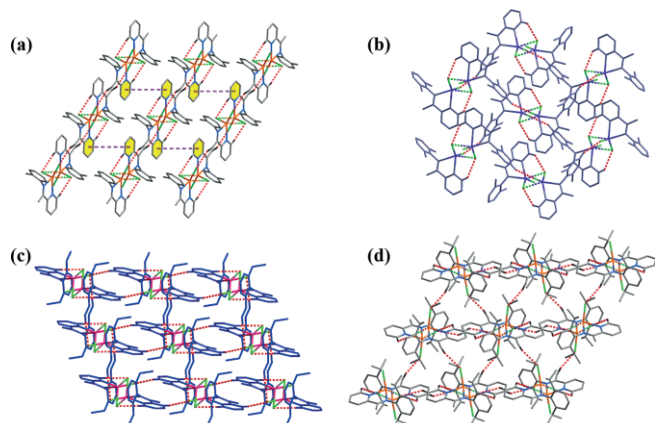


Figure 3. The 2D layer structures in (a) Hg2a, (b) Hg4a, (c) Hg5a, and (d) Hg6a. The dotted lines represent the C–H...Cl and  $\pi$ – $\pi$  interactions.

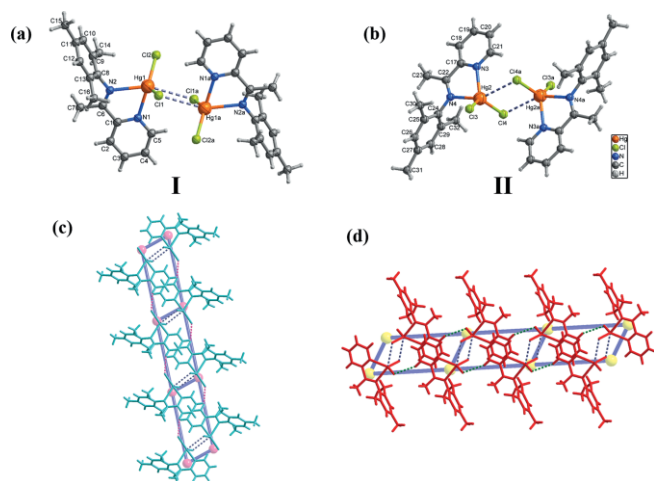


Figure 4. Molecular structure of Hg7a showing the crystallographic numbering schemes of (a) I and (b) II. The 1D arrangements of (c) I and (d) II type molecules (different colors are used to distinguish I and II).

H5A...Cl1 (2.709 Å), C18-H18A...Cl3 (2.815 Å), and C21-H21A...Cl4 (2.669 Å) hydrogen bonds to form two different 1D ladder-shaped chains, as shown in Figure 5 (c and d). As shown in Figure S13, C-H... $\pi$  interactions in Hg2a, Hg4a, and Hg6b provide further stabilization. The details of the C-H...Cl hydrogen-bond,  $\pi$ - $\pi$  stacking, and C-H... $\pi$  interactions for Hg1a-Hg7a are summarized in Table S4.

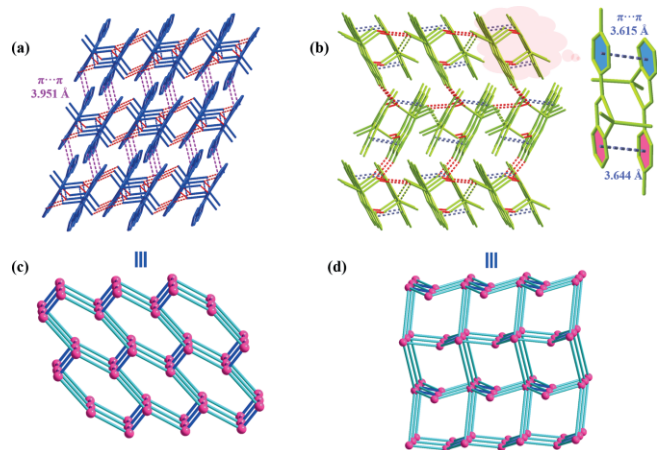


Figure 5. The 3D network structures in (a) Hg1b and (b) Hg3b. The dotted lines represent the C-H...Cl and  $\pi$ - $\pi$  interactions. Topological views of the 3D network structures of (c) Hg1b and (d) Hg3b.

### Structural Analysis of Hg1b-Hg7b

The structures of Hg2b-Hg7b were determined in the present study and reveal a variety of structural motifs; the structure of Hg1b was briefly reported previously but is included in the discussion here for completeness. The crystallographic data for Hg1b-Hg7b are listed in Table S1. Selected bond lengths and angles are summarized in Tables S2 and S3. After recrystallization from *n*-hexane, yellow block crystals of ligands L3b and L6b were obtained. The N2-C6 bond lengths of 1.262(2) Å (L3b) and 1.263(1) Å (L6b) indicate C=N double-bond character.<sup>[22]</sup> The N1-C1-C6-N2 torsion angles of 12(3)/-4(3)° (Hg3b) and -4.4(6)° (Hg6b) are twisted compared with those for the free ligands L3b [-176.9(17)°] and L6b [-176.5(14)°], as shown in Table S5. This can be explained by the stabilization of the structure through the coordination interaction. As shown in Figures 2 (b) and S14, secondary Hg...Cl interactions exist in all of these structures except for Hg3b, and the corresponding Hg...Cl distances are listed in Table 1. In Hg1b, Hg2b, and Hg4b-Hg6b, the Hg cations are in pseudo-square-pyramidal coordination environments with  $\tau_5$  values in the range 0.017-0.291 (Table 1). However, in Hg7b, the Hg cation is in a pseudo-trigonal-bipyramidal environment ( $\tau_5 = 0.508$ ) with atoms N1, Cl1, and Cl2 in the equatorial positions and the axial sites occupied by atoms N2 and Cl1a. An interesting result was obtained for Hg3b, namely, two independent [HgL3bCl<sub>2</sub>] molecules were found. The Hg1...Cl4 distance of 3.559 Å is above the sum of the van der Waals radii (1.70 + 1.80 = 3.50 Å); thus, the coordination geometries around the Hg1 and Hg2 atoms can be better described as trigonal pyramidal ( $\tau_4 = 0.751$ )<sup>[23]</sup> and pseudo-square-pyramidal ( $\tau_5 = 0.263$ ), respectively. The Hg...Hg distances of 4.042-4.636 Å show no weak d<sup>10</sup>...d<sup>10</sup> interactions.

The pyridyl and phenyl rings of the corresponding ligands in Hg1b and Hg3b are arranged in a nearly parallel fashion (11.760 vs. 7.152/7.860°). Nevertheless, in Hg2b and Hg4b-Hg7b, the dihedral angles between the pyridyl and phenyl rings are twisted compared with those in Hg1b and Hg3b. Supramolecular structure analyses revealed that the mononuclear units of Hg1b-Hg7b are further connected into 3D networks (in Hg1b and Hg3b) and 1D chains (in Hg2b and Hg4b-Hg7b) through noncovalent interactions, such as C-H...Cl/ $\pi$ - $\pi$  and secondary Hg...Cl interactions. Clearly, these results show that the substituents play critical roles in directing the supramolecular assemblies of these complexes. The details of the C-H...Cl hydrogen bonds and  $\pi$ - $\pi$  stacking interactions for the complexes Hg1b-Hg7b are summarized in Table S4. As shown in Figure 5 (a), the mononuclear [HgL1bCl<sub>2</sub>] units are linked by intermolecular C-H...Cl hydrogen-bond interactions (the H5A...Cl1, H5A...Cl2, and H6A...Cl2 distances are 2.914, 2.893, and 2.900 Å, respectively) and secondary Hg...Cl interactions with a distance of 2.881 Å to form a 2D layer structure. Then, the 2D layers further extend into 3D five-connected bnn supramolecular structures through  $\pi$ - $\pi$  stacking interactions (3.951 Å). In Hg3b, in addition to  $\pi$ - $\pi$  stacking interactions, intermolecular C-H...Cl and secondary Hg...Cl interactions assemble the mononuclear molecules into a 3D supramolecular network (Figure 5, b). The overall topologies of Hg1b and Hg3b can be reduced to 3D architectures with point symbols (4<sup>6</sup>.6<sup>4</sup>) and (6<sup>9</sup>.8), as illustrated in Figure 5 (c and d), respectively. In contrast to Hg1b and Hg3b, complexes Hg2b and Hg4b-Hg7b only form 1D chains (Figure S15) owing to the steric effects of the substituents. The C-H... $\pi$  interactions in Hg4b-Hg7b also provide further stabilization (Figure S16).

### Photoluminescence Studies

#### Absorption and Solution Luminescence Properties of the Mercury(II) Complexes in CH<sub>3</sub>CN

The UV/Vis absorption spectra of Hg1a-Hg7a and Hg1b-Hg7b in CH<sub>3</sub>CN (10  $\mu$ mol L<sup>-1</sup>) were recorded at room temperature (Figure 6). As the molecules have similar structures, the UV/Vis spectra are similar. All of the spectra exhibit two distinct absorption bands in the range  $\lambda = 250$  to 450 nm ( $\epsilon = 2962$ -45710 M<sup>-1</sup> cm<sup>-1</sup>). The maximum absorption wavelengths and molar extinction coefficients ( $\epsilon$ ) are listed in Table 2. The high-energy bands at  $\lambda \approx 274$ -285 nm are assigned to the  $\pi$ - $\pi^*$  transitions of the C=N chromophores, whereas the low-energy bands at  $\lambda \approx 330$ -360 nm are attributed to n- $\pi^*$  transitions,<sup>[24]</sup> in accordance with previous studies of Schiff base complexes. The introduction of electron-donating groups (-CH<sub>3</sub> in the aldehyde or alkyl groups in the aniline) results in slight bathochromic shifts of the absorption bands.

Upon excitation in the UV domain ( $\lambda \approx 340$  nm), the fourteen complexes give rise to blue luminescence. The excitation spectra of Hg1a-Hg7a and Hg1b-Hg7b are dominated by two intense bands centered at  $\lambda = 275$  nm and  $\lambda \approx 350$ -370 nm, respectively (Figure S17). Excitation at the maximum of the low-energy excitation band resulted in the observation of emission bands with maxima at  $\lambda = 413$ -428 and 401-425 nm for Hg1a-

Table 2. Photophysical properties of Hg1a–Hg7a, Hg1b–Hg7b.

| Complex | Absorption <sup>[a]</sup>   |  | Photoluminescence in acetonitrile |                            |           |                          | Photoluminescence in the solid state |                            |                            |           |                          |
|---------|-----------------------------|--|-----------------------------------|----------------------------|-----------|--------------------------|--------------------------------------|----------------------------|----------------------------|-----------|--------------------------|
|         | $\lambda_{\text{abs}}$ [nm] | $(\epsilon, \text{M}^{-1} \text{cm}^{-1})$ | $\lambda_{\text{ex}}$ [nm]        | $\lambda_{\text{em}}$ [nm] | FWHM [nm] | $\tau$ [ $\mu\text{s}$ ] | $\Phi_{\text{PL}}^{\text{[b]}}$      | $\lambda_{\text{ex}}$ [nm] | $\lambda_{\text{em}}$ [nm] | FWHM [nm] | $\tau$ [ $\mu\text{s}$ ] |
| Hg1a    | 279 (22615), 346 (4436)     |  | 366                               | 413                        | 68.98     | 5.27                     | 0.012                                | 390                        | 454                        | 112.75    | 8.91                     |
| Hg2a    | 283 (23503), 354 (7516)     |  | 374                               | 425                        | 66.29     | 7.28                     | 0.019                                | 384                        | 456                        | 114.68    | 9.09                     |
| Hg3a    | 285 (33380), 356 (2962)     |  | 375                               | 428                        | 79.29     | 7.23                     | 0.022                                | 373                        | 456                        | 103.36    | 8.00                     |
| Hg4a    | 285 (42395), 356 (7845)     |  | 374                               | 425                        | 61.32     | 7.01                     | 0.028                                | 388                        | 480                        | 128.18    | 9.23                     |
| Hg5a    | 284 (26510), 360 (4410)     |  | 373                               | 423                        | 66.87     | 6.69                     | 0.020                                | 380                        | 470                        | 115.10    | 7.82                     |
| Hg6a    | 283 (45710), 356 (19490)    |  | 374                               | 426                        | 66.17     | 7.27                     | 0.018                                | 368                        | 465                        | 134.20    | 7.73                     |
| Hg7a    | 285 (33160), 360 (14440)    |  | 374                               | 428                        | 68.68     | 7.29                     | 0.033                                | 396                        | 494                        | 126.15    | 7.77                     |
| Hg1b    | 275 (15089), 330 (3067)     |  | 349                               | 406                        | 58.99     | 4.03                     | 0.029                                | 351                        | 443                        | 143.72    | 8.25                     |
| Hg2b    | 280 (29977), 336 (12742)    |  | 340                               | 402                        | 58.49     | 4.65                     | 0.021                                | 358                        | 456                        | 149.38    | 7.47                     |
| Hg3b    | 283 (32280), 331 (27135)    |  | 340                               | 425                        | 60.21     | 8.64                     | 0.040                                | 383                        | 480                        | 74.41     | 9.71                     |
| Hg4b    | 282 (14865), 346 (5505)     |  | 339                               | 401                        | 61.49     | 4.96                     | 0.022                                | 378                        | 472                        | 105.96    | 7.45                     |
| Hg5b    | 274 (27172), 340 (3697)     |  | 342                               | 416                        | 68.99     | 7.48                     | 0.016                                | 358                        | 469                        | 132.78    | 9.53                     |
| Hg6b    | 274 (32910), 340 (3922)     |  | 339                               | 411                        | 63.20     | 5.44                     | 0.018                                | 347                        | 466                        | 153.32    | 7.26                     |
| Hg7b    | 281 (29760), 345 (12757)    |  | 339                               | 416                        | 65.67     | 4.88                     | 0.025                                | 352                        | 482                        | 145.84    | 7.13                     |

[a] Measured in CH<sub>3</sub>CN solution (ca.  $1 \times 10^{-5}$  M). [b] Quinine sulfate in 0.1 mol L<sup>-1</sup> H<sub>2</sub>SO<sub>4</sub> as reference ( $\Phi_{\text{PL}} = 0.546$ ,  $\lambda_{\text{ex}} = 350$  nm).

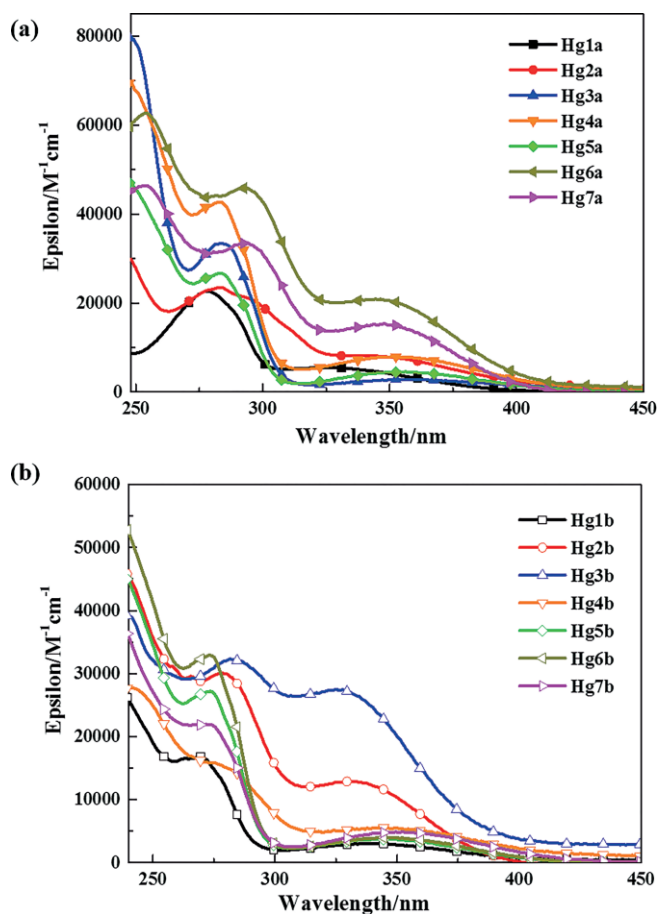


Figure 6. UV/Vis absorption spectra of (a) Hg1a–Hg7a and (b) Hg1b–Hg7b in acetonitrile solution at room temperature.

Hg7a and Hg1b–Hg7b, respectively, (Figure 7, a and b). These bands exhibit blue luminescence, as shown in Figure 7, c and d, and the Commission Internationale d'Eclairage (CIE) coordinates are summarized in Table S6. The effects of the ligand structure on the luminescence properties will be discussed in detail below. In general, the complexes are weakly emissive in CH<sub>3</sub>CN solution, and their luminescence quantum yield values

( $\Phi_{\text{F}}$ ) are in the range 0.012–0.040 (Table 2), as measured with quinine sulfate as a reference ( $\Phi_{\text{PL}} = 0.546$  at  $\lambda = 350$  nm); this may be related to the heavy-atom effect.<sup>[25]</sup> However, Hg1b and Hg3b exhibit moderately strong emission yields, which may be derived from the better planarity of the Schiff base ligands in these complexes (dihedral angles: 11.760° for Hg1b, 7.152 and 7.860° for Hg3b).

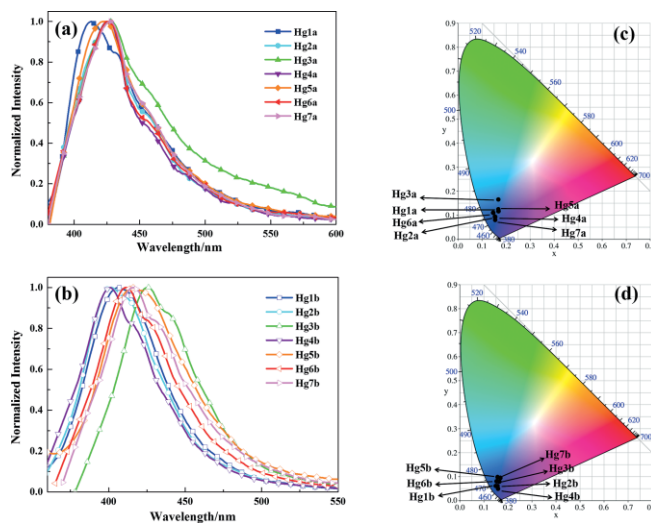


Figure 7. Emission spectra of (a) Hg1a–Hg7a and (b) Hg1b–Hg7b in acetonitrile solution at 298 K. CIE chromaticity diagrams (1931 CIE standard) for (c) Hg1a–Hg7a and (d) Hg1b–Hg7b.

### Solid-State Luminescence Properties of the Mercury(II) Complexes

The emission data for Hg1a–Hg7a and Hg1b–Hg7b in the solid state are summarized in Table 2. Upon excitation at  $\lambda \approx 350$  nm (Figure S18), Hg1a–Hg7a display light blue emission with maxima at  $\lambda = 454, 456, 456, 480, 470, 465,$  and  $494$  nm, respectively (Figures 8, a, and S19). These emission bands can be assigned to the  $\pi^*-\pi$  transitions of the corresponding Schiff base ligands.<sup>[26]</sup> The electron-donating ability of the substituents varies in the order  $\text{H} < i\text{-C}_3\text{H}_7 < \text{C}_2\text{H}_5 < \text{CH}_3$ , and the emission wavelength of the complexes varies in the order Hg1a

(H) < Hg2a (2-CH<sub>3</sub>), Hg3a (4-CH<sub>3</sub>) < Hg4a [2,6-(CH<sub>3</sub>)<sub>2</sub>] < Hg7a [2,4,6-(CH<sub>3</sub>)<sub>3</sub>], and Hg6a [2,6-(*i*-C<sub>3</sub>H<sub>7</sub>)<sub>2</sub>] < Hg5a [2,6-(C<sub>2</sub>H<sub>5</sub>)<sub>2</sub>] < Hg4a [2,6-(CH<sub>3</sub>)<sub>2</sub>], according to the classification of the substituents. The electron-donating effect decreased the energy difference between the highest occupied molecular orbital (HOMO) and the lowest unoccupied molecular orbital (LUMO) and led to redshifted  $\lambda_{Em}$ .<sup>[27]</sup> The emission spectra of Hg1b–Hg7b also reveal this trend with maxima at  $\lambda = 443, 456, 480, 472, 469, 466,$  and  $482$  nm, respectively (Figure 8, b). In this study, we successfully synthesized two sets of complexes, that is, those with “–CMe=N–” moieties and those with “–CH=N–” moieties. We found that the former (Hg1a–Hg7a) have longer emission wavelengths than the latter (Hg1b–Hg7b) owing to the introduction of a –CH<sub>3</sub> group to the aldehyde. This confirms that the different substituents have an influence on the electronic structure and produce different optical properties. Interestingly, Hg3b emits bright blue-green luminescence at  $\lambda_{Em} = 480$  nm when irradiated at  $\lambda = 365$  nm (inset of Figure 8, b). This phenomenon can be explained by the better planarity of L3b in complex Hg3b.<sup>[28]</sup> In the solid state, the maxima of the emission wavelengths for the mercury(II) complexes are redshifted compared with those in acetonitrile solutions; this may be caused by the formation of C–H...Cl hydrogen bonds and  $\pi$ – $\pi$  stacking interactions in the solid state, which can effectively decrease the HOMO–LUMO energy gap and influence the ligand-centered  $\pi^*-\pi$  transitions.<sup>[29]</sup> Meanwhile, the full width at half-maximum (FWHM) values of the emission bands increase from the solid state to acetonitrile solution (Table 2).

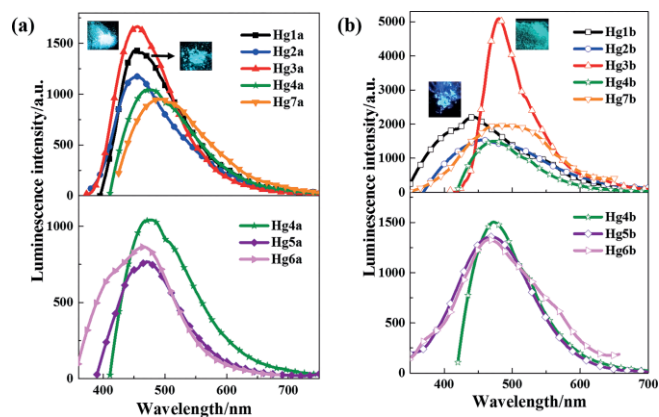


Figure 8. Emission spectra of (a) Hg1a–Hg7a and (b) Hg1b–Hg7b in the solid state at 298 K.

In addition, the luminescence decay profiles of Hg1a–Hg7a and Hg1b–Hg7b (Figures S20–S21) were investigated. The emission lifetimes for Hg1a–Hg7a and Hg1b–Hg7b are in the microsecond range (Table S7). These values indicate that the heavy-atom effect (chlorine) on the molecular skeleton induces a higher intersystem crossing (ISC) efficiency, which results in a decrease of the emission from the singlet state owing to the population of the triplet state.<sup>[30]</sup> Low-temperature measurements of the emission spectra at 77 K were necessary to further confirm this hypothesis. Compared with emission spectra at 298 K, the emission spectra at 77 K (Figures S22–S23) are redshifted by ca. 25–113 nm. The detailed data are listed in

Table S8. This emission spectra of frozen solutions (77 K) of the complexes demonstrate that the luminescence of the complexes is triplet-based.<sup>[31]</sup> A general trend is that the emission lifetime in the solid state ( $\tau = 7.73$ – $9.23$   $\mu$ s for Hg1a–Hg7a;  $\tau = 7.13$ – $9.71$   $\mu$ s for Hg1b–Hg7b) is longer than that in CH<sub>3</sub>CN solution ( $\tau = 5.27$ – $7.29$   $\mu$ s for Hg1a–Hg7a;  $\tau = 4.03$ – $8.64$   $\mu$ s for Hg1b–Hg7b); this might be explained by the occurrence of additional nonradiative deactivation processes in CH<sub>3</sub>CN solution.<sup>[32]</sup>

### AIE Properties of Hg1a, Hg3a, Hg1b, and Hg3b

Among the fourteen complexes, Hg1a, Hg3a, Hg1b, and Hg3b exhibit naked-eye-visible brilliant blue emission in the solid state when irradiated with UV light (insets of Figure 8) but they show very weak emission in CH<sub>3</sub>CN. These complexes are soluble in common organic solvents such as chloroform, dimethyl sulfoxide, and acetonitrile but insoluble in water. A different amount of water ( $f_w$  in the range 0–90 %) was titrated gradually to the acetonitrile solutions of Hg1a, Hg3a, Hg1b, and Hg3b with the overall concentration of the solution kept at  $10 \mu\text{mol L}^{-1}$ . Interestingly, the luminescence intensities of Hg1a, Hg3a, Hg1b, and Hg3b were enhanced and exhibited spectral shifts owing to their aggregated nature. Hence, we proceeded to analyze the AIE further.

As shown in Figure 9, upon the titration of water ( $f_w$  from 0 to 90 %) into acetonitrile solutions of Hg1a, Hg3a, Hg1b, and Hg3b, the luminescence peaks were gradually enhanced and redshifted. Plots of the emission enhancement versus  $f_w$  are depicted in the insets of Figure 9. The emission intensities in the CH<sub>3</sub>CN/H<sub>2</sub>O mixtures with  $f_w = 90$  % are ca. 14.1, 13.2, 15.2, and 38.9 times higher than those in pure CH<sub>3</sub>CN solution for Hg1a, Hg3a, Hg1b, and Hg3b, respectively; therefore, these complexes have AIE activity. Moreover, the increasing luminescence intensity of these complexes with a redshift was caused by the aggregation effect, and the luminescence band of Hg1a shifted from  $\lambda = 413$  to 423 nm ( $428 \rightarrow 440$  nm, Hg3a;

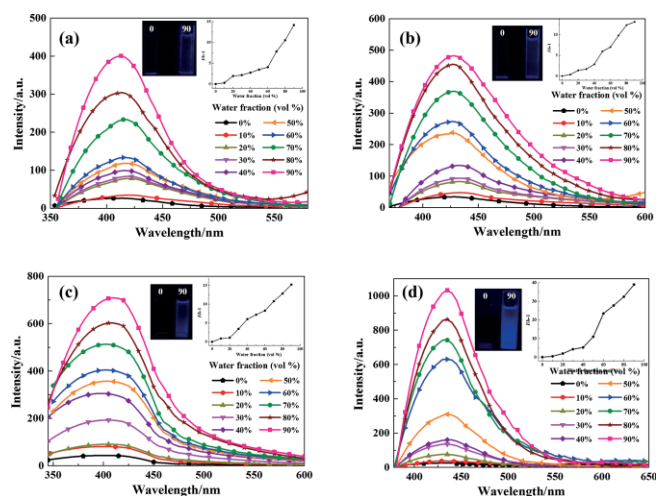


Figure 9. Changes in emission intensities of (a) Hg1a, (b) Hg3a, (c) Hg1b, and (d) Hg3b ( $10 \mu\text{M}$ ) in CH<sub>3</sub>CN solutions titrated with water (0–90 % v/v) at room temperature. Inset: Plot of  $I/I_0 - 1$  versus  $f_w$ ;  $I_0$  is the PL intensity in pure CH<sub>3</sub>CN solution; photos of complexes ( $f_w = 0$  and 90 % v/v) under UV illumination (365 nm).

406→424 nm, Hg**1b**; 425→442 nm, Hg**3b**). Compared with the emission spectra of Hg**1a**, Hg**3a**, Hg**1b**, and Hg**3b** in CH<sub>3</sub>CN solution, the solid emission spectra show redshifted emission by 28–55 nm, and the solid-state emission intensities of these four complexes are at least ten times (11.3, Hg**1a**; 12.5, Hg**3a**; 10.5, Hg**1b**; 25.9, Hg**3b**) higher than those in pure CH<sub>3</sub>CN solution (Figure S24).

We performed another experiment in which the emission spectra of Hg**1a**, Hg**3a**, Hg**1b**, and Hg**3b** at different concentrations in CH<sub>3</sub>CN were recorded (Figure S25). It can be clearly seen that the CH<sub>3</sub>CN solutions with low concentrations ( $c = 10^{-5}$  M) were almost nonemissive, and the fluorescence spectra were nearly parallel to the abscissa. However, the fluorescence intensities increased abruptly when the concentrations were higher than  $10^{-3}$  M. As the concentrations reached  $10^{-1}$  M, the emission intensities were approximately 8.4–18.9 times higher than for the molecularly dispersed species in CH<sub>3</sub>CN for Hg**1a**, Hg**3a**, Hg**1b**, and Hg**3b**. The emission maxima were redshifted by 19–35 nm. These results indicate that these complexes are indeed weak emitters in dilute solution and exhibit properties close to those described for the aggregation-induced emission concept.<sup>[33]</sup> As reported previously,<sup>[34]</sup> the AIE mechanism of these complexes possibly arises from the restriction of intramolecular rotation. In the CH<sub>3</sub>CN/H<sub>2</sub>O (10:90 v/v) mixture, most of the molecules aggregate together rapidly through the intermolecular C–H...Cl hydrogen bonding and  $\pi$ – $\pi$  stacking interactions between adjacent pyridyl and phenyl rings, such that free rotations are hindered and the rigidity of the molecules is increased further to generate a more extended planar skeleton, which might influence the luminescence.<sup>[35]</sup> However, our observations of AIE in the luminescence spectra of Hg**1a**, Hg**3a**, Hg**1b**, and Hg**3b** suggests that both the enhancement and redshift caused by aggregation probably originate from the suppression of twisted intramolecular charge transfer. The above justification was also well supported by similar reports of AIE.<sup>[36]</sup> As shown in Table 2, Hg**1a** and Hg**3a** have twisted conformations with larger torsion angles between the pyridyl and phenyl rings (78.786 and 72.279°, respectively) than those of Hg**1b** and Hg**3b** (11.760 and 7.152/7.860°, respectively). The distorted conformations decrease the planarity and conjugation of the whole molecules and, thus, boost the energy level of the excited state. As a result, Hg**1a** and Hg**3a** exhibit weaker AIE behavior than Hg**1b** and Hg**3b**. Complexes with these AIE effects can be applied extensively as solid-state emission materials.

## Conclusions

Two series of Schiff base ligands, (*E*)-*N*-(pyridine-2-yl)(CMe=NPhR) and (*E*)-*N*-(pyridine-2-yl)(CH=NPhR), were used to synthesize fourteen mercury(II) complexes Hg**1a**–Hg**7a** and Hg**1b**–Hg**7b**. These complexes are excellent models for investigating the effects of the alkyl substituents [–H, 2-CH<sub>3</sub>, 4-CH<sub>3</sub>, 2,6-(CH<sub>3</sub>)<sub>2</sub>, 2,6-(C<sub>2</sub>H<sub>5</sub>)<sub>2</sub>, 2,6-(*i*-C<sub>3</sub>H<sub>7</sub>)<sub>2</sub>, and 2,4,6-(CH<sub>3</sub>)<sub>3</sub>] on the supramolecular metal–organic frameworks (SMOFs) and their photoluminescence properties. The crystal structures of these complexes indicate that intermolecular interactions, such as secondary Hg...Cl, C–H...Cl hydrogen-bond, and  $\pi$ – $\pi$  interactions, play

essential roles in the construction of 1D to 3D supramolecular structures. This study clearly demonstrated that –H and 4-CH<sub>3</sub> substituents in the phenyl ring can lead to 3D supramolecular structures (Hg**1a**, Hg**3a**, Hg**1b**, and Hg**3b**), whereas large substituents such as 2-CH<sub>3</sub>, 2,6-(CH<sub>3</sub>)<sub>2</sub>, 2,6-(C<sub>2</sub>H<sub>5</sub>)<sub>2</sub>, 2,6-(*i*-C<sub>3</sub>H<sub>7</sub>)<sub>2</sub>, and 2,4,6-(CH<sub>3</sub>)<sub>3</sub> readily form 2D (Hg**2a**, Hg**4a**–Hg**6a**) or 1D (Hg**7a**, Hg**2b**, Hg**4b**–Hg**7b**) SMOFs. Upon irradiation with UV light, Hg**1a**–Hg**7a** and Hg**1b**–Hg**7b** display deep blue emission at  $\lambda = 401$ –428 nm in acetonitrile solution and light blue emissions at  $\lambda = 443$ –494 nm in the solid state. The photoluminescence properties of mercury(II) Schiff base complexes can be tuned finely and predictably over a wide range of wavelengths through small and readily implemented changes to the ligand structure. By modifying the phenyl moiety with electron-donating substituents, the energy difference between the HOMO and LUMO decreases, and the emissions are redshifted accordingly. It is worth noting that Hg**1a**, Hg**3a**, Hg**1b**, and Hg**3b** exhibit good aggregation-induced emission (AIE) properties in CH<sub>3</sub>CN/H<sub>2</sub>O mixtures; in particular, the emission intensity of Hg**3b** with  $f_w = 90$  % is ca. 39.9 times higher than that in pure CH<sub>3</sub>CN.

## Experimental Section

**Materials and Instrumentation: Caution!** Compounds of mercury are extremely toxic, and appropriate handling conditions should be used for their generation and disposal. All reagents and solvents were purchased from commercial sources and used without further purification. Elemental analyses were performed with a Perkin–Elmer 2400 automatic analyzer. The FTIR spectra (4000–400 cm<sup>–1</sup>) were recorded with a Nicolet impact 410 FTIR spectrometer. The <sup>1</sup>H NMR spectra were obtained with a Bruker Avance 400 MHz spectrometer with Si(CH<sub>3</sub>)<sub>4</sub> as an internal standard. The <sup>13</sup>C NMR (150 MHz) spectra were recorded with a Bruker Avance-600 spectrometer. The MS (ESI) spectra were recorded with a Bruker Esquire LC mass spectrometer. The PXRD patterns were recorded in the  $2\theta$  range 5–50° with Cu-K $\alpha$  radiation with a Shimadzu XRD-6000 X-ray diffractometer. A Perkin–Elmer Lambda 35 spectrometer was used to record the UV/Vis absorption spectra of the ligands and complexes. The emission luminescence and lifetime properties were recorded with an Edinburgh Instruments FLS 920 fluorescence spectrometer. Lifetime studies were performed with a photon-counting system with a microsecond pulse lamp as the excitation source. The emission decays were analyzed by the sum of exponential functions. The decay curves were fitted to a double exponential function:<sup>[37]</sup>  $I(t) = A_1 \exp(-t/\tau_1) + A_2 \exp(-t/\tau_2)$ , in which  $I$  is the luminescence intensity, and  $\tau_1$  and  $\tau_2$  are the lifetimes for the exponential components. The average lifetimes were calculated with Equation (1).

$$\frac{\tau_1^2 A_1 \% + \tau_2^2 A_2 \%}{\tau_1 A_1 \% + \tau_2 A_2 \%} \quad (1)$$

Quinine sulfate in 0.1 M H<sub>2</sub>SO<sub>4</sub> (quantum yield 0.54 at 350 nm) was chosen as the standard.<sup>[38]</sup> The absolute values were calculated from the fixed and known fluorescence quantum yield of the standard reference sample through Equation (2).

$$Q = Q_R \frac{I}{I_R} \frac{OD_R}{OD} \frac{n^2}{n_R^2} \quad (2)$$

In Equation (2),  $Q$  is the quantum yield,  $I$  is the measured integrated emission intensity,  $n$  is the refractive index, and OD is the optical

density. The subscript *R* refers to the reference fluorophore of known quantum yield. To minimize reabsorption effects, absorbencies in the 10 mm fluorescence cuvette were kept under 0.05 at the excitation wavelength (350 nm).

**X-ray Crystallography:** Suitable crystals of **L3b**, **L6b**, **Hg1a–Hg7a**, and **Hg1b–Hg7b** were selected, mounted, and studied with a Rigaku R-Axis RAPID IP diffractometer. The diffraction data were collected with graphite-monochromated Mo- $K_{\alpha}$  radiation ( $\lambda = 0.71073 \text{ \AA}$ ). The structures were solved with direct methods<sup>[39]</sup> and refined with full-matrix least-squares techniques on  $F^2$ . All hydrogen atoms were constrained in geometric positions to their parent atoms, and non-hydrogen atoms were refined anisotropically. The detailed crystal structure refinement data are given in Table S1, and selected bond lengths and angles are listed in Tables S2 and S3.

CCDC 1442117 (for **Hg1a**), 1442118 (for **Hg2a**), 1442119 (for **Hg3a**), 1442120 (for **Hg4a**), 1442121 (for **Hg5a**), 1442122 (for **Hg6a**), 1442123 (for **Hg7a**), 1442124 (for **Hg2b**), 1442125 (for **Hg3b**), 1442126 (for **Hg4b**), 1442127 (for **Hg5b**), 1442128 (for **Hg6b**), 1442129 (for **Hg7b**), 1442130 (for **L3b**), and 1442131 (for **L6b**) contain the supplementary crystallographic data for this paper. These data can be obtained free of charge from The Cambridge Crystallographic Data Centre.

**General Synthesis of Ligands:** 2-Acetylpyridine in anhydrous methanol (10 mL) and the respective aniline derivative (aniline, 2-methylaniline, 4-methylaniline, 2,6-dimethylaniline, 2,6-diethylaniline, 2,6-diisopropylaniline, or 2,4,6-trimethylaniline; 1 equiv.) in anhydrous methanol (10 mL) were mixed. The resultant solutions were heated under reflux for ca. 8–12 h and subsequently concentrated under reduced pressure to obtain **L1a–L7a** as brown oil-like crude products. The procedure for **L1b–L7b** was similar to that for **L1a–L7a**, except that 2-pyridinecarbaldehyde was used instead of 2-acetylpyridine. Ligands **L1b** and **L2b** were yellow oils, and **L3b–L7b** were yellow powders. Ligands **L3b** and **L6b** were recrystallized from *n*-hexane/dichloromethane and *n*-hexane to afford yellow crystals.

**N-[(Pyridin-2-yl)ethylidene]aniline (L1a):** 2-Acetylpyridine (1.58 mL, 14.13 mmol) and aniline (1.29 mL, 14.15 mmol) afforded the product (2.53 g, yield 91 %).  $C_{13}H_{12}N_2$  (196.25): calcd. C 79.56, H 6.16, N 14.27; found C 79.61, H 6.15, N 14.23. FTIR (KBr):  $\tilde{\nu} = 3434$  (w), 3070 (w), 2962 (m), 2871 (w), 1625 (s), 1586 (m), 1567 (w), 1460 (s), 1438 (s), 1385 (m), 1297 (w), 1282 (m), 1265 (m), 1238 (m), 1146 (w), 1117 (w), 1101 (w), 1057 (w), 1044 (m), 995 (w), 956 (w), 885 (w), 824 (w), 780 (m), 745 (m), 590 (w), 533 (w)  $cm^{-1}$ .  $^1H$  NMR (400 MHz,  $CDCl_3$ ):  $\delta = 8.72$  (d, 1 H, Py- $H^6$ ), 8.09 (d, 1 H, Py- $H^3$ ), 7.86 (m, 1 H, Py- $H^4$ ), 7.50 (m, 1 H, Py- $H^5$ ), 6.84–7.19 (m, 5 H, Ph- $H^{2,3,4,5,6}$ ), 2.77 (s, 3 H,  $CH_3$ ) ppm.  $^{13}C$  NMR (150 MHz,  $CDCl_3$ ):  $\delta = 167.31$ , 153.45, 148.95, 146.53, 136.85, 129.22, 127.13, 121.60, 118.33, 115.03, 16.40 ppm. MS (ESI):  $m/z = 196.63$  [M + H] $^+$ .

**(E)-2-Methyl-N-[(pyridin-2-yl)ethylidene]aniline (L2a):** 2-Acetylpyridine (1.27 mL, 11.33 mmol) and 2-methylaniline (1.21 mL, 11.31 mmol) afforded the product (2.11 g, yield 89 %).  $C_{14}H_{14}N_2$  (210.28): calcd. C 79.97, H 6.71, N 13.32; found C 80.03, H 6.74, N 13.29. FTIR (KBr):  $\tilde{\nu} = 3433$  (w), 3056 (w), 2918 (w), 2860 (w), 1643 (s), 1624 (m), 1584 (m), 1568 (w), 1499 (m), 1468 (m), 1437 (m), 1358 (s), 1299 (m), 1282 (s), 1239 (m), 1222 (w), 1190 (w), 1148 (w), 1102 (m), 1043 (m), 995 (w), 955 (w), 927 (w), 837 (w), 781 (s), 743 (s), 716 (w), 623 (w), 591 (m), 537 (w)  $cm^{-1}$ .  $^1H$  NMR (400 MHz,  $CDCl_3$ ):  $\delta = 8.71$  (d, 1 H, Py- $H^6$ ), 8.08 (d, 1 H, Py- $H^3$ ), 7.84 (m, 1 H, Py- $H^4$ ), 7.48 (m, 1 H, Py- $H^5$ ), 6.68–7.08 (m, 4 H, Ph- $H^{2,3,4,5,6}$ ), 2.77 (s, 3 H,  $CH_3$ ), 2.19 (s, 3 H, Ph- $CH_3$ ) ppm.  $^{13}C$  NMR (150 MHz,  $CDCl_3$ ):  $\delta = 166.89$ , 153.55, 149.02, 148.58, 144.80, 136.88, 130.44, 127.17, 126.98,

121.64, 118.47, 114.90, 17.82, 16.56 ppm. MS (ESI):  $m/z = 211.12$  [M + H] $^+$ .

**(E)-4-Methyl-N-[(pyridin-2-yl)ethylidene]aniline (L3a):** 2-Acetylpyridine (1.57 mL, 14.00 mmol) and 4-methylaniline (1.56 mL, 14.00 mmol) afforded the product (2.25 g, yield 76 %).  $C_{14}H_{14}N_2$  (210.28): calcd. C 79.97, H 6.71, N 13.32; found C 79.94, H 6.75, N 13.35. FTIR (KBr):  $\tilde{\nu} = 3433$  (w), 3054 (w), 2921 (w), 2862 (w), 1639 (s), 1584 (m), 1568 (m), 1517 (s), 1506 (s), 1466 (m), 1436 (m), 1358 (s), 1298 (m), 1282 (s), 1239 (m), 1219 (m), 1179 (w), 1149 (w), 1104 (s), 1044 (m), 1019 (w), 995 (m), 955 (m), 843 (m), 815 (m), 782 (m), 743 (w), 709 (w), 621 (w), 590 (m), 575 (w), 507 (m)  $cm^{-1}$ .  $^1H$  NMR (400 MHz,  $CDCl_3$ ):  $\delta = 8.72$  (d, 1 H, Py- $H^6$ ), 8.08 (d, 1 H, Py- $H^3$ ), 7.86 (m, 1 H, Py- $H^4$ ), 7.50 (m, 1 H, Py- $H^5$ ), 6.64–7.00 (m, 4 H, Ph- $H^{2,3,4,5,6}$ ), 2.76 (s, 3 H,  $CH_3$ ), 2.26 (s, 3 H, Ph- $CH_3$ ) ppm.  $^{13}C$  NMR (150 MHz,  $CDCl_3$ ):  $\delta = 162.47$ , 158.96, 149.91, 143.78, 137.67, 129.74, 127.79, 122.36, 119.66, 115.26, 20.45, 16.36 ppm. MS (ESI):  $m/z = 211.12$  [M + H] $^+$ .

**(E)-2,6-Dimethyl-N-[(pyridin-2-yl)ethylidene]aniline (L4a):** 2-Acetylpyridine (1.09 mL, 9.71 mmol) and 2,6-dimethylaniline (1.20 mL, 9.73 mmol) afforded the product (1.76 g, yield 81 %).  $C_{15}H_{16}N_2$  (224.31): calcd. C 80.32, H 7.19, N 12.49; found C 80.27, H 7.18, N 12.52. FTIR (KBr):  $\tilde{\nu} = 3436$  (w), 3053 (w), 2919 (w), 2855 (w), 1650 (s), 1584 (w), 1569 (w), 1478 (m), 1437 (m), 1357 (m), 1297 (w), 1282 (m), 1239 (m), 1148 (w), 1100 (m), 1044 (w), 995 (w), 954 (w), 897 (w), 780 (m), 760 (m), 738 (w), 683 (w), 623 (w), 590 (m), 544 (w), 491 (w)  $cm^{-1}$ .  $^1H$  NMR (400 MHz,  $CDCl_3$ ):  $\delta = 8.72$  (d, 1 H, Py- $H^6$ ), 8.06 (d, 1 H, Py- $H^3$ ), 7.85 (m, 1 H, Py- $H^4$ ), 7.49 (m, 1 H, Py- $H^5$ ), 6.67–6.98 (m, 3 H, Ph- $H^{3,4,5}$ ), 2.77 (s, 3 H,  $CH_3$ ), 2.21 (s, 6 H, Ph- $CH_3$ ) ppm.  $^{13}C$  NMR (150 MHz,  $CDCl_3$ ):  $\delta = 167.20$ , 153.46, 148.93, 142.77, 136.78, 128.19, 127.88, 127.06, 121.54, 117.84, 17.55, 16.61 ppm. MS (ESI):  $m/z = 225.14$  [M + H] $^+$ .

**(E)-2,6-Diethyl-N-[(pyridin-2-yl)ethylidene]aniline (L5a):** 2-Acetylpyridine (1.44 mL, 12.86 mmol) and 2,6-diethylaniline (2.14 mL, 12.89 mmol) afforded the product (2.77 g, yield 85 %).  $C_{17}H_{20}N_2$  (252.36): calcd. C 80.91, H 7.99, N 11.10; found C 80.88, H 7.87, N 11.16. FTIR (KBr):  $\tilde{\nu} = 3434$  (w), 3056 (w), 2934 (w), 2873 (w), 1653 (s), 1583 (m), 1569 (w), 1456 (s), 1357 (s), 1297 (m), 1282 (s), 1239 (m), 1149 (w), 1101 (m), 1059 (w), 1043 (w), 1020 (w), 996 (w), 954 (w), 901 (w), 780 (m), 744 (m), 622 (w), 590 (m), 539 (w), 474 (w)  $cm^{-1}$ .  $^1H$  NMR (400 MHz,  $CDCl_3$ ):  $\delta = 8.75$  (d, 1 H, Py- $H^6$ ), 8.12 (d, 1 H, Py- $H^3$ ), 7.86 (m, 1 H, Py- $H^4$ ), 7.50 (m, 1 H, Py- $H^5$ ), 6.81–7.05 (m, 3 H, Ph- $H^{3,4,5}$ ), 2.81 (s, 3 H,  $CH_3$ ), 2.61 (q, 4 H, Ph- $CH_2$ ), 1.33 (t, 6 H, Ph- $CH_3$ ) ppm.  $^{13}C$  NMR (150 MHz,  $CDCl_3$ ):  $\delta = 166.91$ , 156.37, 153.50, 148.93, 141.61, 136.73, 127.48, 125.95, 121.51, 118.18, 24.25, 16.96, 13.02 ppm. MS (ESI):  $m/z = 253.17$  [M + H] $^+$ .

**(E)-2,6-Diisopropyl-N-[(pyridin-2-yl)ethylidene]aniline (L6a):** 2-Acetylpyridine (0.96 mL, 8.58 mmol) and 2,6-diisopropylaniline (1.61 mL, 8.56 mmol) afforded the product (1.95 g, yield 81 %).  $C_{19}H_{24}N_2$  (280.41): calcd. C 81.38, H 8.63, N 9.99; found C 81.44, H 8.65, N 9.96. FTIR (KBr):  $\tilde{\nu} = 3435$  (w), 3072 (w), 2925 (w), 2863 (w), 1655 (s), 1603 (s), 1586 (m), 1568 (m), 1500 (s), 1484 (w), 1467 (m), 1437 (m), 1421 (w), 1358 (m), 1298 (w), 1283 (m), 1239 (m), 1216 (w), 1174 (w), 1102 (m), 1075 (w), 1044 (m), 1028 (w), 995 (m), 955 (m), 906 (w), 879 (w), 780 (m), 754 (m), 694 (m), 623 (w), 591 (m), 506 (m)  $cm^{-1}$ .  $^1H$  NMR (400 MHz,  $CDCl_3$ ):  $\delta = 8.71$  (d, 1 H, Py- $H^6$ ), 8.08 (d, 1 H, Py- $H^3$ ), 7.85 (m, 1 H, Py- $H^4$ ), 7.49 (m, 1 H, Py- $H^5$ ), 6.78–7.17 (m, 3 H, Ph- $H^{3,4,5}$ ), 2.76 (s, 3 H,  $CH_3$ ), 2.25 (q, 2 H, Ph- $CH$ ), 1.28 (d, 12 H, Ph- $CH_3$ ) ppm.  $^{13}C$  NMR (150 MHz,  $CDCl_3$ ):  $\delta = 166.95$ , 156.42, 148.57, 136.48, 135.77, 124.79, 123.58, 122.98, 122.75, 121.32, 28.24, 23.22, 22.90, 17.32 ppm. MS (ESI):  $m/z = 281.18$  [M + H] $^+$ .

**(E)-2,4,6-Trimethyl-N-[(pyridin-2-yl)ethylidene]aniline (L7a):** 2-Acetylpyridine (1.43 mL, 12.73 mmol) and 2,4,6-trimethylaniline (1.78 mL, 12.71 mmol) afforded the product (2.80 g, yield 92 %).  $C_{16}H_{18}N_2$  (238.33): calcd. C 80.63, H 7.61, N 11.75; found C 80.68, H 7.67, N 11.70. FTIR (KBr):  $\tilde{\nu}$  = 3436 (w), 3053 (w), 2922 (w), 2861 (w), 1657 (s), 1608 (w), 1584 (w), 1568 (w), 1492 (s), 1467 (w), 1437 (m), 1378 (w), 1357 (s), 1297 (m), 1282 (m), 1239 (m), 1215 (w), 1157 (w), 1101 (m), 1043 (w), 1012 (w), 995 (w), 954 (w), 856 (m), 780 (s), 742 (w), 622 (w), 590 (m), 561 (w)  $cm^{-1}$ .  $^1H$  NMR (400 MHz,  $CDCl_3$ ):  $\delta$  = 8.72 (d, 1 H, Py- $H^6$ ), 8.08 (d, 1 H, Py- $H^3$ ), 7.85 (m, 1 H, Py- $H^4$ ), 7.49 (m, 1 H, Py- $H^5$ ), 6.80 (s, 2 H, Ph- $H^{3,5}$ ), 2.77 (s, 3 H,  $CH_3$ ), 2.21 (t, 9 H, Ph- $CH_3$ ) ppm.  $^{13}C$  NMR (150 MHz,  $CDCl_3$ ):  $\delta$  = 162.47, 158.96, 149.91, 143.78, 137.67, 129.74, 127.79, 122.36, 119.66, 115.26, 20.45, 16.36 ppm. MS (ESI):  $m/z$  = 239.16 [M + H] $^+$ .

**N-[(Pyridin-2-yl)methylene]aniline (L1b):** 2-Pyridinecarbaldehyde (0.68 mL, 7.15 mmol) and aniline (0.65 mL, 7.13 mmol) afforded the product (1.17 g, yield 90 %).  $C_{12}H_{10}N_2$  (182.22): calcd. C 79.10, H 5.53, N 15.37; found C 79.15, H 5.49, N 15.32. FTIR (KBr):  $\tilde{\nu}$  = 3340 (w), 3052 (w), 2960 (w), 2857 (w), 1650 (m), 1600 (s), 1570 (w), 1502 (m), 1471 (w), 1432 (m), 1319 (m), 1276 (w), 1251 (w), 1200 (w), 1178 (w), 1149 (w), 1087 (w), 1072 (w), 1045 (w), 1027 (w), 993 (m), 975 (w), 910 (w), 873 (w), 813 (w), 811 (w), 779 (m), 752 (s), 694 (m), 663 (w), 619 (w), 580 (w), 538 (w), 512 (w)  $cm^{-1}$ .  $^1H$  NMR (400 MHz,  $CDCl_3$ ):  $\delta$  = 8.72 (d, 1 H, Py- $H^6$ ), 8.61 (s, 1 H, CH=N), 8.22 (d, 1 H, Py- $H^3$ ), 7.81 (t, 1 H, Py- $H^4$ ), 7.63 (t, 1 H, Py- $H^5$ ), 6.61–7.42 (m, 5 H, Ph- $H^{2,3,4,5,6}$ ) ppm.  $^{13}C$  NMR (150 MHz,  $CDCl_3$ ):  $\delta$  = 160.60, 154.51, 149.68, 136.70, 129.22, 126.72, 121.09, 117.54, 115.05, 113.01 ppm. MS (ESI):  $m/z$  = 183.09 [M + H] $^+$ .

**(E)-2-Methyl-N-[(pyridin-2-yl)methylene]aniline (L2b):** 2-Pyridinecarbaldehyde (1.44 mL, 15.14 mmol) and 2-methylaniline (1.62 mL, 15.16 mmol) afforded the product (2.69 g, yield 91 %).  $C_{13}H_{12}N_2$  (196.25): calcd. C 79.56, H 6.16, N 14.27; found C 79.52, H 6.20, N 14.23. FTIR (KBr):  $\tilde{\nu}$  = 3349 (w), 3054 (m), 2948 (w), 2858 (w), 1669 (m), 1587 (m), 1567 (m), 1486 (m), 1465 (m), 1436 (m), 1376 (w), 1344 (w), 1305 (w), 1278 (w), 1253 (w), 1211 (m), 1187 (m), 1147 (w), 1112 (m), 1089 (w), 1043 (m), 993 (m), 977 (w), 939 (w), 881 (m), 854 (w), 779 (s), 754 (m), 742 (m), 717 (m), 659 (w), 620 (w), 576 (w), 553 (w), 501 (w)  $cm^{-1}$ .  $^1H$  NMR (400 MHz,  $CDCl_3$ ):  $\delta$  = 8.72 (d, 1 H, Py- $H^6$ ), 8.52 (s, 1 H, CH=N), 8.27 (d, 1 H, Py- $H^3$ ), 7.82 (t, 1 H, Py- $H^4$ ), 7.37 (t, 1 H, Py- $H^5$ ), 7.00–7.24 (m, 4 H, Ph- $H^{3,4,5,6}$ ), 2.39 (s, 3 H, Ph- $CH_3$ ) ppm.  $^{13}C$  NMR (150 MHz,  $CDCl_3$ ):  $\delta$  = 159.79, 154.74, 149.98, 149.50, 136.61, 132.23, 130.35, 126.79, 126.38, 125.02, 121.60, 117.51, 17.85 ppm. MS (ESI):  $m/z$  = 197.11 [M + H] $^+$ .

**(E)-4-Methyl-N-[(pyridin-2-yl)methylene]aniline (L3b):** 2-Pyridinecarbaldehyde (1.52 mL, 15.98 mmol) and 4-methylaniline (1.77 mL, 15.88 mmol) were dissolved in anhydrous methanol (20 mL), and the resulting mixture was heated under reflux for 3 h. The solvent was removed under reduced pressure, and the residue was recrystallized from *n*-hexane/dichloromethane to give yellow crystals, yield 2.79 g (90 %).  $C_{13}H_{12}N_2$  (196.25): calcd. C 79.56, H 6.16, N 14.27; found C 79.55, H 6.17, N 14.28. FTIR (KBr):  $\tilde{\nu}$  = 3429 (w), 3050 (w), 2917 (w), 2861 (w), 1628 (m), 1582 (m), 1566 (m), 1506 (s), 1463 (m), 1434 (m), 1347 (w), 1291 (w), 1256 (w), 1234 (w), 1213 (w), 1198 (w), 1140 (w), 1111 (w), 1085 (w), 1038 (w), 992 (m), 969 (w), 947 (w), 880 (m), 822 (s), 774 (w), 738 (m), 706 (w), 646 (w), 617 (m), 542 (m), 497 (w), 477 (w)  $cm^{-1}$ .  $^1H$  NMR (400 MHz,  $CDCl_3$ ):  $\delta$  = 8.74 (d, 1 H, Py- $H^6$ ), 8.65 (s, 1 H, CH=N), 8.24 (d, 1 H, Py- $H^3$ ), 7.84 (t, 1 H, Py- $H^4$ ), 7.40 (t, 1 H, Py- $H^5$ ), 6.63–7.29 (m, 4 H, Ph- $H^{3,4,5,6}$ ), 2.41 (s, 3 H, Ph- $CH_3$ ) ppm.  $^{13}C$  NMR (150 MHz,  $CDCl_3$ ):  $\delta$  = 159.63, 154.68, 149.63, 148.31, 136.81, 136.71, 129.87, 125.01, 121.82, 121.12, 21.08 ppm. MS (ESI):  $m/z$  = 197.11 [M + H] $^+$ .

**(E)-2,6-Dimethyl-N-[(pyridin-2-yl)methylene]aniline (L4b):** 2-Pyridinecarbaldehyde (1.50 mL, 15.77 mmol) and 2,6-dimethylaniline (1.95 mL, 15.77 mmol) afforded the product (2.72 g, yield 82 %).  $C_{14}H_{14}N_2$  (210.27): calcd. C 79.97, H 6.71, N 13.32; found C 79.90, H 6.67, N 13.42. FTIR (KBr):  $\tilde{\nu}$  = 3434 (w), 3045 (w), 2916 (m), 2852 (w), 1652 (s), 1585 (m), 1568 (m), 1469 (s), 1436 (m), 1374 (w), 1348 (w), 1289 (w), 1252 (w), 1190 (s), 1146 (m), 1088 (m), 1041 (m), 990 (m), 918 (w), 872 (m), 829 (w), 776 (s), 739 (w), 704 (w), 630 (w), 611 (w), 564 (w), 467 (w)  $cm^{-1}$ .  $^1H$  NMR (400 MHz,  $CDCl_3$ ):  $\delta$  = 8.76 (d, 1 H, Py- $H^6$ ), 8.38 (s, 1 H, CH=N), 8.33 (d, 1 H, Py- $H^3$ ), 7.88 (t, 1 H, Py- $H^4$ ), 7.44 (t, 1 H, Py- $H^5$ ), 7.01–7.12 (m, 3 H, Ph- $H^{3,4,5}$ ), 2.20 (s, 6 H, Ph- $CH_3$ ) ppm.  $^{13}C$  NMR (150 MHz,  $CDCl_3$ ):  $\delta$  = 163.44, 154.39, 150.29, 149.60, 136.67, 128.11, 126.79, 125.31, 124.05, 121.18, 18.28 ppm. MS (ESI):  $m/z$  = 211.12 [M + H] $^+$ .

**(E)-2,6-Diethyl-N-[(pyridin-2-yl)methylene]aniline (L5b):** 2-Pyridinecarbaldehyde (1.53 mL, 16.08 mmol) and 2,6-diethylaniline (2.70 mL, 16.28 mmol) afforded the product (3.50 g, yield 91 %).  $C_{16}H_{18}N_2$  (238.33): calcd. C 80.63, H 7.61, N 11.75; found C 80.58, H 7.63, N 11.72. FTIR (KBr):  $\tilde{\nu}$  = 3425 (w), 3052 (w), 2964 (m), 2871 (w), 1643 (s), 1584 (m), 1565 (m), 1468 (s), 1435 (m), 1374 (m), 1355 (w), 1319 (w), 1292 (w), 1256 (w), 1228 (w), 1189 (m), 1164 (w), 1147 (m), 1099 (m), 1088 (w), 1060 (w), 1041 (w), 1006 (w), 992 (m), 964 (w), 875 (s), 835 (w), 797 (w), 775 (s), 753 (s), 704 (w), 635 (w), 618 (w), 593 (w), 563 (w), 525 (w), 499 (w), 471 (w)  $cm^{-1}$ .  $^1H$  NMR (400 MHz,  $CDCl_3$ ):  $\delta$  = 8.78 (d, 1 H, Py- $H^6$ ), 8.38 (s, 1 H, CH=N), 8.32 (d, 1 H, Py- $H^3$ ), 7.89 (t, 1 H, Py- $H^4$ ), 7.45 (t, 1 H, Py- $H^5$ ), 7.09–7.15 (m, 3 H, Ph- $H^{3,4,5}$ ), 2.56 (q, 4 H, Ph- $CH_2$ ), 1.18 (t, 6 H, Ph- $CH_3$ ) ppm.  $^{13}C$  NMR (150 MHz,  $CDCl_3$ ):  $\delta$  = 163.03, 154.40, 149.64, 149.57, 136.74, 132.75, 126.29, 125.33, 124.30, 121.22, 24.66, 14.65 ppm. MS (ESI):  $m/z$  = 239.16 [M + H] $^+$ .

**(E)-2,6-Diisopropyl-N-[(pyridin-2-yl)methylene]aniline (L6b):** 2-Pyridinecarbaldehyde (1.16 mL, 12.19 mmol) was heated under reflux (4 h) with 2,6-diisopropylaniline (2.35 mL, 12.46 mmol) in anhydrous methanol (25 mL). The solvent was removed under reduced pressure, and the residue was purified by column chromatography with ethyl acetate/petroleum ether (1:3 v/v) as the eluent. Recrystallization from *n*-hexane gave yellow crystals, which were collected by filtration and washed with cold *n*-hexane, yield 2.28 g (70 %).  $C_{18}H_{22}N_2$  (266.38): calcd. C 81.16, H 8.32, N 10.52; found C 81.08, H 8.36, N 10.50. FTIR (KBr):  $\tilde{\nu}$  = 3428 (w), 3072 (w), 2959 (vs), 2867 (m), 16553 (s), 1587 (m), 1567 (m), 1471 (s), 1440 (m), 1385 (m), 1363 (m), 1347 (w), 1324 (m), 1308 (w), 1295 (m), 1254 (m), 1226 (w), 1179 (m), 1150 (m), 1107 (w), 1091 (w), 1054 (m), 1045 (m), 1011 (w), 996 (m), 970 (w), 933 (m), 879 (m), 827 (w), 808 (w), 796 (m), 779 (m), 755 (s), 701 (w), 640 (w), 620 (w), 563 (w), 533 (w), 493 (w), 459 (w)  $cm^{-1}$ .  $^1H$  NMR (400 MHz,  $CDCl_3$ ):  $\delta$  = 8.77 (d, 1 H, Py- $H^6$ ), 8.36 (s, 1 H, CH=N), 8.32 (d, 1 H, Py- $H^3$ ), 7.92 (t, 1 H, Py- $H^4$ ), 7.46 (t, 1 H, Py- $H^5$ ), 6.83–7.20 (m, 3 H, Ph- $H^{3,4,5}$ ), 3.00 (q, 2 H, Ph-CH), 1.21 (d, 12 H, Ph- $CH_3$ ) ppm.  $^{13}C$  NMR (150 MHz,  $CDCl_3$ ):  $\delta$  = 162.94, 154.31, 149.67, 148.36, 137.22, 136.77, 125.34, 124.48, 123.05, 121.34, 27.93, 23.46 ppm. MS (ESI):  $m/z$  = 267.19 [M + H] $^+$ .

**(E)-2,4,6-Trimethyl-N-[(pyridin-2-yl)methylene]aniline (L7b):** 2-Pyridinecarbaldehyde (1.50 mL, 15.75 mmol) and 2,4,6-trimethylaniline (2.22 mL, 15.81 mmol) afforded the product (2.68 g, yield 76 %).  $C_{15}H_{16}N_2$  (224.30): calcd. C 80.32, H 7.19, N 12.49; found C 80.28, H 7.18, N 12.45. FTIR (KBr):  $\tilde{\nu}$  = 3432 (w), 3050 (w), 2911 (m), 2854 (w), 1668 (vs), 1586 (m), 1567 (m), 1482 (s), 1468 (s), 1436 (m), 1400 (w), 1386 (w), 1376 (w), 1347 (w), 1288 (w), 1259 (w), 1202 (s), 1144 (m), 1088 (w), 1041 (w), 1015 (w), 993 (m), 982 (m), 955 (w), 934 (w), 897 (w), 876 (s), 863 (s), 791 (m), 770 (s), 739 (m), 643 (w), 618 (w), 577 (w), 489 (w)  $cm^{-1}$ .  $^1H$  NMR (400 MHz,  $CDCl_3$ ):  $\delta$  = 8.72 (d, 1 H, Py- $H^6$ ), 8.33 (s, 1 H, CH=N), 8.29 (d, 1 H, Py- $H^3$ ), 7.84 (t, 1 H,

Py- $H^4$ ), 7.40 (t, 1 H, Py- $H^5$ ), 6.90 (s, 2 H, Ph- $H^{3,5}$ ), 2.14–2.29 (m, 9 H, Ph- $CH_3$ ) ppm.  $^{13}C$  NMR (150 MHz,  $CDCl_3$ ):  $\delta$  = 163.41, 154.52, 149.58, 147.83, 136.68, 133.44, 128.81, 126.84, 125.23, 121.17, 20.75, 18.24 ppm. MS (ESI):  $m/z$  = 225.14 [M + H] $^+$ .

**General Synthesis of Mercury(II) Complexes:** The mercury(II) complexes were synthesized by dissolving  $HgCl_2$  and the respective Schiff base ligand (1 equiv.) in anhydrous solutions. Methanol was used for Hg1a–Hg7a, whereas methanol/dichloromethane mixtures were used for Hg1b–Hg7b, Scheme 1. The yellow solutions were heated under reflux for 12 h and subsequently filtered. Quality single crystals of the fourteen mercury(II) complexes were grown through the slow evaporation of their solutions.

**Complex Hg1a:** Yield 30.1 mg (64%).  $C_{13}H_{12}Cl_2HgN_2$  (467.75): calcd. C 33.38, H 2.59, N 5.99; found C 33.45, H 2.57, N 5.63. FTIR (KBr):  $\tilde{\nu}$  = 3434 (w), 3064 (w), 2962 (w), 2860 (w), 1620 (m), 1591 (m), 1483 (m), 1439 (m), 1372 (m), 1312 (m), 1253 (m), 1212 (m), 1169 (w), 1122 (w), 1102 (w), 1072 (w), 1052 (w), 1027 (w), 1010 (m), 986 (w), 961 (w), 903 (w), 830 (m), 790 (s), 741 (m), 692 (m), 637 (w), 576 (w), 438 (w)  $cm^{-1}$ .  $^1H$  NMR (400 MHz,  $CDCl_3$ ):  $\delta$  = 8.80 (d, 1 H, Py- $H^6$ ), 8.15 (d, 1 H, Py- $H^3$ ), 7.80 (m, 1 H, Py- $H^4$ ), 7.55 (m, 1 H, Py- $H^5$ ), 6.79–7.41 (m, 5 H, Ph- $H^{2,3,4,5,6}$ ), 2.50 (s, 3 H,  $CH_3$ ) ppm.  $^{13}C$  NMR (150 MHz,  $CDCl_3$ ):  $\delta$  = 165.18, 150.16, 148.77, 146.74, 140.09, 137.22, 129.70, 128.13, 125.84, 120.70, 18.16 ppm. MS (ESI):  $m/z$  = 468.11 [M + H] $^+$ , 196.93 [L + H] $^+$ .

**Complex Hg2a:** Yield 28.2 mg (64%).  $C_{14}H_{14}Cl_2HgN_2$  (481.77): calcd. C 34.90, H 2.93, N 5.81; found C 34.95, H 2.85, N 5.77. FTIR (KBr):  $\tilde{\nu}$  = 3434 (w), 3050 (w), 2917 (w), 2852 (w), 1634 (m), 1591 (s), 1572 (w), 1485 (m), 1456 (w), 1437 (m), 1371 (m), 1312 (m), 1254 (s), 1223 (m), 1191 (w), 1166 (w), 1126 (w), 1113 (w), 1102 (w), 1054 (w), 1045 (w), 1015 (m), 986 (w), 943 (w), 844 (w), 804 (m), 778 (s), 755 (m), 717 (w), 639 (w), 576 (w), 539 (w), 441 (w)  $cm^{-1}$ .  $^1H$  NMR (400 MHz,  $CDCl_3$ ):  $\delta$  = 8.82 (d, 1 H, Py- $H^6$ ), 8.11 (d, 1 H, Py- $H^3$ ), 7.81 (m, 1 H, Py- $H^4$ ), 7.52 (m, 1 H, Py- $H^5$ ), 6.71–7.24 (m, 4 H, Ph- $H^{3,4,5,6}$ ), 2.40 (s, 3 H,  $CH_3$ ), 2.21 (s, 3 H, Ph- $CH_3$ ) ppm.  $^{13}C$  NMR (150 MHz,  $CDCl_3$ ):  $\delta$  = 165.86, 150.00, 149.02, 139.88, 136.96, 131.16, 130.47, 128.03, 127.22, 126.31, 125.65, 119.79, 18.02, 17.38 ppm. MS (ESI):  $m/z$  = 482.60 [M + H] $^+$ , 211.12 [L + H] $^+$ .

**Complex Hg3a:** Yield 29.0 mg (60%).  $C_{14}H_{14}Cl_2HgN_2$  (481.77): calcd. C 34.90, H 2.93, N 5.81; found C 34.96, H 2.99, N 5.78. FTIR (KBr):  $\tilde{\nu}$  = 3433 (w), 3068 (w), 2916 (w), 2859 (w), 1635 (m), 1591 (s), 1574 (w), 1502 (s), 1477 (w), 1440 (m), 1366 (m), 1315 (m), 1254 (m), 1217 (m), 1171 (m), 1118 (w), 1105 (w), 1053 (w), 1011 (m), 988 (w), 940 (w), 850 (m), 830 (w), 788 (s), 748 (w), 707 (w), 634 (w), 575 (w), 522 (w), 446 (w)  $cm^{-1}$ .  $^1H$  NMR (400 MHz,  $CDCl_3$ ):  $\delta$  = 8.77 (d, 1 H, Py- $H^6$ ), 8.06 (d, 1 H, Py- $H^3$ ), 7.85 (m, 1 H, Py- $H^4$ ), 7.48 (m, 1 H, Py- $H^5$ ), 6.62–7.05 (m, 4 H, Ph- $H^{2,3,5,6}$ ), 2.48 (s, 3 H,  $CH_3$ ), 2.38 (s, 3 H, Ph- $CH_3$ ) ppm.  $^{13}C$  NMR (150 MHz,  $CDCl_3$ ):  $\delta$  = 164.88, 150.15, 144.08, 140.09, 136.62, 130.23, 128.06, 125.78, 120.79, 115.99, 21.06, 18.10 ppm. MS (ESI):  $m/z$  = 482.60 [M + H] $^+$ , 211.12 [L + H] $^+$ .

**Complex Hg4a:** Yield 29.4 mg (59%).  $C_{15}H_{16}Cl_2HgN_2$  (495.80): calcd. C 36.34, H 3.25, N 5.65; found C 36.41, H 3.30, N 5.60. FTIR (KBr):  $\tilde{\nu}$  = 3435 (w), 3066 (w), 2917 (w), 2853 (w), 1642 (m), 1591 (s), 1574 (w), 1470 (w), 1437 (m), 1370 (w), 1311 (m), 1252 (m), 1202 (m), 1164 (w), 1120 (w), 1095 (w), 1052 (w), 1035 (w), 1013 (m), 982 (w), 923 (w), 893 (w), 836 (w), 795 (s), 777 (s), 739 (w), 703 (w), 640 (w), 629 (w), 586 (w), 559 (w), 541 (w), 499 (w), 438 (w)  $cm^{-1}$ .  $^1H$  NMR (400 MHz,  $CDCl_3$ ):  $\delta$  = 8.84 (d, 1 H, Py- $H^6$ ), 8.14 (d, 1 H, Py- $H^3$ ), 7.83 (m, 1 H, Py- $H^4$ ), 7.52 (m, 1 H, Py- $H^5$ ), 7.10–7.17 (m, 3 H, Ph- $H^{3,4,5}$ ), 2.36 (s, 3 H,  $CH_3$ ), 2.20 (s, 6 H, Ph- $CH_3$ ) ppm.  $^{13}C$  NMR (150 MHz,  $CDCl_3$ ):  $\delta$  = 166.48, 150.24, 149.10, 145.00, 140.23, 137.20, 128.84, 127.67, 126.13, 122.19, 18.46, 17.77 ppm. MS (ESI):  $m/z$  = 496.95 [M + H] $^+$ , 225.14 [L + H] $^+$ .

**Complex Hg5a:** Yield 35.3 mg (67%).  $C_{17}H_{20}Cl_2HgN_2$  (523.85): calcd. C 38.98, H 3.85, N 5.35; found C 38.89, H 3.91, N 5.40. FTIR (KBr):  $\tilde{\nu}$  = 3427 (w), 3055 (w), 2958 (w), 2869 (w), 1644 (m), 1594 (m), 1571 (w), 1440 (m), 1367 (m), 1315 (m), 1253 (m), 1195 (m), 1170 (m), 1124 (w), 1103 (w), 105 (w), 985 (w), 906 (w), 871 (w), 836 (w), 811 (w), 777 (s), 742 (w), 705 (w), 640 (w), 565 (w), 534 (w), 435 (w)  $cm^{-1}$ .  $^1H$  NMR (400 MHz,  $CDCl_3$ ):  $\delta$  = 8.80 (d, 1 H, Py- $H^6$ ), 8.13 (d, 1 H, Py- $H^3$ ), 7.79 (m, 1 H, Py- $H^4$ ), 7.49 (m, 1 H, Py- $H^5$ ), 7.19–7.24 (m, 3 H, Ph- $H^{3,4,5}$ ), 2.66 (s, 3 H,  $CH_3$ ), 2.37 (q, 4 H, Ph- $CH_2$ ), 1.18 (t, 6 H, Ph- $CH_3$ ) ppm.  $^{13}C$  NMR (150 MHz,  $CDCl_3$ ):  $\delta$  = 166.82, 153.46, 149.98, 144.09, 139.94, 136.93, 132.93, 128.14, 126.04, 121.78, 23.83, 18.28, 13.68 ppm. MS (ESI):  $m/z$  = 524.65 [M + H] $^+$ , 253.17 [L + H] $^+$ .

**Complex Hg6a:** Yield 33.9 mg (61%).  $C_{19}H_{24}Cl_2HgN_2$  (551.89): calcd. C 41.35, H 4.38, N 5.08; found C 41.38, H 4.44, N 5.01. FTIR (KBr):  $\tilde{\nu}$  = 3432 (w), 3069 (w), 2963 (w), 2868 (w), 1633 (m), 1591 (s), 1574 (w), 1482 (w), 1463 (m), 1443 (m), 1386 (m), 1370 (m), 1326 (w), 1312 (m), 1256 (s), 1187 (m), 1164 (m), 1121 (m), 1104 (w), 1056 (m), 1045 (w), 1016 (s), 986 (w), 937 (w), 836 (w), 813 (m), 797 (m), 784 (s), 746 (w), 701 (w), 636 (w), 575 (w), 459 (w), 434 (w)  $cm^{-1}$ .  $^1H$  NMR (400 MHz,  $CDCl_3$ ):  $\delta$  = 8.84 (d, 1 H, Py- $H^6$ ), 8.16 (d, 1 H, Py- $H^3$ ), 7.83 (m, 1 H, Py- $H^4$ ), 7.55 (m, 1 H, Py- $H^5$ ), 7.15–7.28 (m, 3 H, Ph- $H^{3,4,5}$ ), 2.72 (s, 3 H,  $CH_3$ ), 2.40 (q, 2 H, Ph- $CH$ ), 1.10–1.32 (m, 12 H, Ph- $CH_3$ ) ppm.  $^{13}C$  NMR (150 MHz,  $CDCl_3$ ):  $\delta$  = 166.93, 150.16, 149.06, 140.21, 138.45, 128.42, 126.90, 124.35, 123.35, 122.14, 28.27, 24.52, 22.83, 19.22 ppm. MS (ESI):  $m/z$  = 552.74 [M + H] $^+$ , 281.18 [L + H] $^+$ .

**Complex Hg7a:** Yield 35.7 mg (70%).  $C_{16}H_{18}Cl_2HgN_2$  (509.83): calcd. C 37.69, H 3.56, N 5.49; found C 37.73, H 3.60, N 5.51. FTIR (KBr):  $\tilde{\nu}$  = 3437 (w), 3060 (w), 2915 (w), 2855 (w), 1644 (m), 1593 (s), 1572 (w), 1479 (m), 1439 (m), 1370 (m), 1315 (m), 1253 (s), 1213 (s), 1168 (w), 1155 (m), 1101 (w), 1053 (w), 1036 (w), 1013 (m), 987 (w), 955 (w), 900 (w), 857 (m), 810 (w), 786 (s), 746 (w), 635 (m), 602 (w), 561 (w), 506 (w), 435 (w)  $cm^{-1}$ .  $^1H$  NMR (400 MHz,  $CDCl_3$ ):  $\delta$  = 8.83 (d, 1 H, Py- $H^6$ ), 8.12 (d, 1 H, Py- $H^3$ ), 7.82 (m, 1 H, Py- $H^4$ ), 7.52 (m, 1 H, Py- $H^5$ ), 6.96 (s, 2 H, Ph- $H^{3,5}$ ), 2.36 (s, 3 H,  $CH_3$ ), 2.16–2.32 (m, 9 H, Ph- $CH_3$ ) ppm.  $^{13}C$  NMR (150 MHz,  $CDCl_3$ ):  $\delta$  = 166.68, 150.19, 142.46, 140.19, 137.12, 129.46, 128.41, 127.41, 125.79, 122.10, 20.83, 18.35, 17.70 ppm. MS (ESI):  $m/z$  = 510.67 [M + H] $^+$ , 239.16 [L + H] $^+$ .

**Complex Hg1b:** Yield 25.0 mg (55%).  $C_{12}H_{10}Cl_2HgN_2$  (453.71): calcd. C 31.77, H 2.22, N 6.17; found C 31.80, H 2.23, N 6.10. FTIR (KBr):  $\tilde{\nu}$  = 3430 (w), 3062 (w), 2952 (w), 2870 (w), 1627 (w), 1590 (s), 1561 (w), 1492 (s), 1475 (m), 1455 (m), 1436 (s), 1418 (w), 1370 (m), 1338 (w), 1305 (m), 1288 (w), 1269 (w), 1240 (m), 1190 (w), 1153 (m), 1099 (m), 1079 (w), 1015 (m), 980 (s), 962 (m), 917 (m), 904 (s), 835 (w), 784 (s), 769 (s), 737 (m), 686 (m), 640 (m), 559 (w), 537 (m), 477 (w), 424 (w)  $cm^{-1}$ .  $^1H$  NMR (400 MHz,  $CDCl_3$ ):  $\delta$  = 8.89 (d, 1 H, Py- $H^6$ ), 8.72 (s, 1 H,  $CH=N$ ), 8.40 (d, 1 H, Py- $H^3$ ), 8.06 (t, 1 H, Py- $H^4$ ), 7.77 (t, 1 H, Py- $H^5$ ), 6.60–7.51 (m, 5 H, Ph- $H^{2,3,4,5,6}$ ) ppm.  $^{13}C$  NMR (150 MHz,  $CDCl_3$ ):  $\delta$  = 166.65, 150.48, 140.62, 139.55, 129.76, 127.51, 121.68, 118.24, 116.28, 115.16 ppm. MS (ESI):  $m/z$  = 454.58 [M + H] $^+$ , 183.09 [L + H] $^+$ .

**Complex Hg2b:** Yield 25.4 mg (52%).  $C_{13}H_{14}Cl_2HgN_2O$  (485.75): calcd. C 32.14, H 2.90, N 5.77; found C 32.10, H 2.95, N 5.70. FTIR (KBr):  $\tilde{\nu}$  = 3433 (w), 3060 (w), 2950 (w), 2860 (w), 1633 (w), 1592 (m), 1565 (w), 1489 (m), 1460 (w), 1439 (m), 1377 (w), 1314 (w), 1265 (w), 1238 (w), 1210 (w), 1184 (w), 1159 (w), 1114 (w), 1050 (w), 1016 (m), 984 (w), 953 (w), 904 (w), 867 (w), 776 (s), 757 (m), 715 (w), 638 (w), 583 (w), 561 (w), 503 (w), 477 (w), 453 (w)  $cm^{-1}$ .  $^1H$  NMR (400 MHz,  $CDCl_3$ ):  $\delta$  = 8.79 (d, 1 H, Py- $H^6$ ), 8.57 (s, 1 H,  $CH=N$ ), 8.21 (d, 1 H, Py- $H^3$ ), 8.06 (t, 1 H, Py- $H^4$ ), 7.64 (t, 1 H, Py- $H^5$ ), 7.13–7.24 (m, 4 H, Ph- $H^{3,4,5,6}$ ), 2.34 (s, 3 H, Ph- $CH_3$ ) ppm.  $^{13}C$  NMR (150 MHz,  $CDCl_3$ ):  $\delta$  = 164.50, 158.68, 155.76, 151.81, 151.43, 142.03,

137.12, 133.29, 127.88, 125.34, 120.35, 119.83, 19.17 ppm. MS (ESI):  $m/z = 486.55 [M + H]^+$ , 197.11 [L + H]<sup>+</sup>.

**Complex Hg3b:** Yield 26.4 mg (57%). C<sub>13</sub>H<sub>12</sub>Cl<sub>2</sub>HgN<sub>2</sub> (467.74): calcd. C 33.38, H 2.59, N 5.99; found C 33.40, H 2.57, N 5.92. FTIR (KBr):  $\tilde{\nu} = 3429$  (w), 3060 (w), 2946 (w), 2856 (w), 1626 (w), 1591 (m), 1562 (m), 1508 (m), 1476 (m), 1440 (m), 1414 (w), 1370 (w), 1320 (w), 1306 (m), 1271 (w), 1236 (w), 1192 (w), 1179 (w), 1154 (w), 1127 (w), 1103 (w), 1059 (w), 1038 (w), 1018 (m), 975 (m), 953 (w), 906 (m), 823 (s), 769 (m), 740 (w), 700 (w), 645 (w), 535 (m), 509 (w), 436 (w) cm<sup>-1</sup>. <sup>1</sup>H NMR (400 MHz, CDCl<sub>3</sub>):  $\delta = 8.90$  (d, 1 H, Py-H<sup>6</sup>), 8.75 (s, 1 H, CH=N), 8.20 (d, 1 H, Py-H<sup>3</sup>), 7.97 (t, 1 H, Py-H<sup>4</sup>), 7.73 (t, 1 H, Py-H<sup>5</sup>), 7.32–7.45 (m, 4 H, Ph-H<sup>2,3,5,6</sup>), 2.37 (s, 3 H, Ph-CH<sub>3</sub>) ppm. <sup>13</sup>C NMR (150 MHz, CDCl<sub>3</sub>):  $\delta = 162.49, 156.63, 150.97, 148.68, 141.08, 140.96, 130.53, 124.11, 121.84, 121.32, 22.36$  ppm. MS (ESI):  $m/z = 468.59 [M + H]^+$ , 197.11 [L + H]<sup>+</sup>.

**Complex Hg4b:** Yield 31.3 mg (65%). C<sub>14</sub>H<sub>14</sub>Cl<sub>2</sub>HgN<sub>2</sub> (481.76): calcd. C 34.90, H 2.93, N 5.81; found C 34.95, H 2.90, N 5.82. FTIR (KBr):  $\tilde{\nu} = 3431$  (w), 3069 (w), 2965 (w), 2853 (w), 1644 (m), 1595 (m), 1571 (w), 1469 (m), 1443 (m), 1386 (w), 1359 (w), 1311 (w), 1267 (w), 1224 (w), 1181 (m), 1158 (w), 1104 (w), 1091 (w), 1058 (w), 1043 (w), 1017 (m), 984 (w), 970 (w), 921 (w), 893 (m), 830 (w), 783 (s), 774 (s), 745 (w), 711 (w), 642 (w), 627 (w), 557 (w), 516 (w), 480 (w), 422 (w) cm<sup>-1</sup>. <sup>1</sup>H NMR (400 MHz, CDCl<sub>3</sub>):  $\delta = 8.86$  (d, 1 H, Py-H<sup>6</sup>), 8.58 (s, 1 H, CH=N), 8.17 (d, 1 H, Py-H<sup>3</sup>), 7.86 (t, 1 H, Py-H<sup>4</sup>), 7.59 (t, 1 H, Py-H<sup>5</sup>), 7.10–7.17 (m, 3 H, Ph-H<sup>3,4,5</sup>), 2.31 (s, 6 H, Ph-CH<sub>3</sub>) ppm. <sup>13</sup>C NMR (150 MHz, CDCl<sub>3</sub>):  $\delta = 166.67, 153.97, 150.14, 142.68, 139.64, 137.11, 128.47, 128.23, 125.63, 121.47, 18.57$  ppm. MS (ESI):  $m/z = 482.52 [M + H]^+$ , 211.12 [L + H]<sup>+</sup>.

**Complex Hg5b:** Yield 34.3 mg (67%). C<sub>16</sub>H<sub>18</sub>Cl<sub>2</sub>HgN<sub>2</sub> (509.81): calcd. C 37.69, H 3.56, N 5.49; found C 37.62, H 3.55, N 5.45. FTIR (KBr):  $\tilde{\nu} = 3424$  (w), 3057 (w), 2967 (w), 2875 (w), 1640 (m), 1591 (s), 1569 (w), 1508 (w), 1476 (m), 1448 (s), 1373 (w), 1342 (w), 1328 (w), 1305 (m), 1268 (w), 1241 (w), 1218 (w), 1175 (m), 1158 (w), 1103 (m), 1053 (w), 1016 (m), 978 (w), 966 (w), 898 (m), 810 (m), 775 (s), 742 (w), 701 (w), 637 (w), 566 (w), 533 (m), 487 (w), 433 (w) cm<sup>-1</sup>. <sup>1</sup>H NMR (400 MHz, CDCl<sub>3</sub>):  $\delta = 8.84$  (d, 1 H, Py-H<sup>6</sup>), 8.53 (s, 1 H, CH=N), 8.13 (d, 1 H, Py-H<sup>3</sup>), 7.82 (t, 1 H, Py-H<sup>4</sup>), 7.55 (t, 1 H, Py-H<sup>5</sup>), 7.16–7.23 (m, 3 H, Ph-H<sup>3,4,5</sup>), 2.65 (q, 4 H, Ph-CH<sub>2</sub>), 1.18 (t, 6 H, Ph-CH<sub>3</sub>) ppm. <sup>13</sup>C NMR (150 MHz, CDCl<sub>3</sub>):  $\delta = 161.94, 150.52, 147.52, 146.58, 139.93, 134.31, 129.12, 128.80, 126.68, 126.41, 24.33, 15.08$  ppm. MS (ESI):  $m/z = 510.61 [M + H]^+$ , 239.16 [L + H]<sup>+</sup>.

**Complex Hg6b:** Yield 27.5 mg (51%). C<sub>18</sub>H<sub>22</sub>Cl<sub>2</sub>HgN<sub>2</sub> (537.87): calcd. C 40.19, H 4.12, N 5.21; found C 40.11, H 4.15, N 5.23. FTIR (KBr):  $\tilde{\nu} = 3425$  (w), 3062 (w), 2963 (m), 2866 (w), 1645 (m), 1592 (s), 1566 (w), 1509 (m), 1477 (m), 1457 (m), 1440 (m), 1384 (w), 1363 (m), 1330 (w), 1307 (m), 1270 (w), 1256 (w), 1240 (w), 1223 (w), 1176 (m), 1155 (w), 1102 (m), 1057 (w), 1043 (w), 1013 (m), 996 (w), 977 (w), 956 (w), 933 (w), 900 (m), 823 (s), 805 (m), 772 (s), 761 (m), 742 (w), 701 (w), 636 (w), 535 (m), 497 (w), 468 (w), 420 (w) cm<sup>-1</sup>. <sup>1</sup>H NMR (400 MHz, CDCl<sub>3</sub>):  $\delta = 8.85$  (d, 1 H, Py-H<sup>6</sup>), 8.51 (s, 1 H, CH=N), 8.15 (d, 1 H, Py-H<sup>3</sup>), 7.85 (t, 1 H, Py-H<sup>4</sup>), 7.55 (t, 1 H, Py-H<sup>5</sup>), 7.24–7.27 (m, 3 H, Ph-H<sup>3,4,5</sup>), 3.12 (q, 2 H, Ph-CH), 1.241 (t, 12 H, Ph-CH<sub>3</sub>) ppm. <sup>13</sup>C NMR (150 MHz, CDCl<sub>3</sub>):  $\delta = 161.18, 150.44, 147.65, 144.95, 139.97, 139.33, 129.07, 128.71, 126.94, 123.90, 28.06, 24.42$  ppm. MS (ESI):  $m/z = 538.87 [M + H]^+$ , 267.19 [L + H]<sup>+</sup>.

**Complex Hg7b:** Yield 32.3 mg (65%). C<sub>15</sub>H<sub>16</sub>Cl<sub>2</sub>HgN<sub>2</sub> (495.79): calcd. C 36.34, H 3.25, N 5.65; found C 36.33, H 3.21, N 5.68. FTIR (KBr):  $\tilde{\nu} = 3433$  (w), 3063 (w), 2913 (w), 2860 (w), 1650 (s), 1594 (m), 1573 (w), 1484 (s), 1445 (m), 1386 (w), 1362 (w), 1310 (m), 1267 (w), 1227 (w), 1200 (s), 1163 (m), 1142 (m), 1103 (w), 1053 (w), 1040 (w), 1016 (m), 979 (w), 965 (w), 934 (w), 892 (m), 867 (m), 822 (w),

777 (s), 740 (w), 638 (m), 582 (w), 534 (w), 514 (w), 493 (w), 459 (w) cm<sup>-1</sup>. <sup>1</sup>H NMR (400 MHz, CDCl<sub>3</sub>):  $\delta = 8.84$  (d, 1 H, Py-H<sup>6</sup>), 8.56 (s, 1 H, CH=N), 8.15 (d, 1 H, Py-H<sup>3</sup>), 7.81 (t, 1 H, Py-H<sup>4</sup>), 7.59 (t, 1 H, Py-H<sup>5</sup>), 6.97 (s, 2 H, Ph-H<sup>3,5</sup>), 2.20–2.33 (m, 9 H, Ph-CH<sub>3</sub>) ppm. <sup>13</sup>C NMR (150 MHz, CDCl<sub>3</sub>):  $\delta = 161.94, 150.40, 147.64, 145.10, 139.89, 136.15, 129.33, 129.09, 128.73, 128.36, 20.84, 18.65$  ppm. MS (ESI):  $m/z = 496.55 [M + H]^+$ , 225.14 [L + H]<sup>+</sup>.

## Acknowledgments

This work was supported by National Natural Science Foundation of China (NSFC) (grant numbers 21371040, 21571042, and 21171044), the National key Basic Research Program of China (973 Program, grant number 2013CB632900).

**Keywords:** Metal–organic frameworks · Hydrogen bonding · Pi interactions · Luminescence · Aggregation-induced emission · Mercury

- [1] a) P. Dechambenoit, S. Ferlay, N. Kyritsakas, M. W. Hosseini, *J. Am. Chem. Soc.* **2008**, *130*, 17106–17113; b) S. Takamizawa, T. Akatsuka, T. Ueda, *Angew. Chem. Int. Ed.* **2008**, *47*, 1689–1692; *Angew. Chem.* **2008**, *120*, 1713–1716; c) M. J. Prakash, S. C. Sevov, *Inorg. Chem.* **2011**, *50*, 12739–12746; d) N. Roques, G. Mouchaham, C. Duhayon, S. Brandès, A. Tachon, G. Weber, J. P. Bellat, J. P. Sutter, *Chem. Eur. J.* **2014**, *20*, 11690–11694; e) L. L. Han, T. P. Hu, K. Mei, Z. M. Guo, C. Yin, Y. X. Wang, J. Zheng, X. P. Wang, D. Sun, *Dalton Trans.* **2015**, *44*, 6052–6061.
- [2] a) K. Hiratani, M. Albrecht, *Chem. Soc. Rev.* **2008**, *37*, 2413–2421; b) M. D. Pluth, R. G. Bergman, K. N. Raymond, *Acc. Chem. Res.* **2009**, *42*, 1650–1659; c) S. A. Barnett, N. R. Champness, *Coord. Chem. Rev.* **2003**, *246*, 145–168; d) G. R. Desiraju, *Angew. Chem. Int. Ed.* **2007**, *46*, 8342–8356; *Angew. Chem.* **2007**, *119*, 8492–8508; e) R. Banerjee, A. Phan, B. Wang, C. Knobler, H. Furukawa, M. O’Keeffe, O. M. Yaghi, *Science* **2008**, *319*, 939–943; f) J. B. Lin, J. P. Zhang, X. M. Chen, *J. Am. Chem. Soc.* **2010**, *132*, 6654–6656; g) S. Yuan, Y. K. Deng, D. Sun, *Chem. Eur. J.* **2014**, *20*, 10093–10098; h) Z. Q. Guo, S. M. Yiu, M. C. W. Chan, *Chem. Eur. J.* **2013**, *19*, 8937–8947.
- [3] a) F. F. B. J. Janssen, R. G. Gelder, A. E. Rowan, *Cryst. Growth Des.* **2011**, *11*, 4326–4333; b) J. S. Field, O. Q. Munro, B. P. Waldron, *Dalton Trans.* **2012**, *41*, 5486–5496; c) J. M. Lin, Y. X. Qiu, W. B. Chen, M. Yang, A. J. Zhou, W. Dong, C. E. Tian, *CrystEngComm* **2012**, *14*, 2779–2786; d) L. He, D. Ma, L. Duan, Y. Wei, J. Qiao, D. Zhang, G. Dong, L. Wang, Y. Qiu, *Inorg. Chem.* **2012**, *51*, 4502–4510; e) R. F. Semeniuc, T. J. Reamer, M. D. Smith, *New J. Chem.* **2010**, *34*, 439–452.
- [4] a) A. Ali, G. Hundal, R. Gupta, *Cryst. Growth Des.* **2012**, *12*, 1308–1319; b) A. Duong, T. Maris, J. D. Wuest, *Inorg. Chem.* **2011**, *50*, 5605–5618; c) D. Natale, J. C. Mareque-Rivas, *Chem. Commun.* **2008**, 425–437; d) M. Nishio, *CrystEngComm* **2004**, *6*, 130–158.
- [5] a) N. W. Alcock, *Structure and Bonding: Structural Principles in Inorganic and Organic Chemistry*, Ellis Horwood, New York, **1990**; b) I. Haiduc, F. T. Edelmann, *Supramolecular Organometallic Chemistry*, Wiley-VCH, Weinheim, Germany, **1999**; c) M. C. Janzen, M. C. Jennings, R. J. Puddephatt, *Inorg. Chem.* **2003**, *42*, 4553–4558; d) G. Berionni, B. Pégot, J. Marrot, R. Goumont, *CrystEngComm* **2009**, *11*, 986–988; e) M. A. Pitt, D. W. Johnson, *Chem. Soc. Rev.* **2007**, *36*, 1441–1453; f) J. Ballmann, S. Dechert, E. Bill, U. Ryde, F. Meyer, *Inorg. Chem.* **2008**, *47*, 1586–159.
- [6] J. Luo, Z. Xie, J. W. Lam, L. Cheng, H. Chen, C. Qiu, H. S. Kwok, X. Zhan, Y. Liu, D. Zhu, B. Z. Tang, *Chem. Commun.* **2001**, 1740–1741.
- [7] a) B. Bhattacharya, R. Haldar, D. K. Maity, T. K. Maji, D. Ghoshal, *CrystEngComm* **2015**, *17*, 3478–3486; b) H. C. Zhou, J. R. Long, O. M. Yaghi, *Chem. Rev.* **2012**, *112*, 673–674; c) W. G. Lu, Z. W. Wei, Z. Y. Gu, T. F. Liu, J. Park, J. Park, J. Tian, M. W. Zhang, Q. Zhang, T. Gentle III, M. Bosch, H. C. Zhou, *Chem. Soc. Rev.* **2014**, *43*, 5561–5593.
- [8] a) G. S. Papaefstathiou, L. R. MacGillivray, *Coord. Chem. Rev.* **2003**, *246*, 169–184; b) I. Kuzu, I. Krummenacher, J. Meyer, F. Armbruster, F. Breher, *Dalton Trans.* **2008**, 5836–5865; c) S. Re, S. Nagase, *Chem. Commun.*

- 2004, 658–659; d) B. H. Northrop, Y. R. Zheng, K. W. Chi, P. J. Stang, *Acc. Chem. Res.* **2009**, *42*, 1554–1563; e) H. R. Khavasi, A. R. Salimi, H. Eshtiagh-Hosseini, M. M. Amini, *CrystEngComm* **2011**, *13*, 3710–3717.
- [9] a) G. F. Li, X. Y. Ren, G. G. Shan, W. L. Che, D. X. Zhu, L. K. Yan, Z. M. Su, M. R. Bryce, *Chem. Commun.* **2015**, *51*, 13036–13039; b) M. Nath, P. K. Saini, *Dalton Trans.* **2011**, *40*, 7077–7121.
- [10] a) V. Stilinović, K. Užarević, I. Cvrtila, B. Kaitner, *CrystEngComm* **2012**, *14*, 7493–7501; b) S. Park, S. Y. Lee, S. S. Lee, *Inorg. Chem.* **2010**, *49*, 1238–1244; c) W. Y. Wong, *Coord. Chem. Rev.* **2007**, *251*, 2400–2427; d) L. Liu, W. Y. Wong, J. X. Shi, K. W. Cheah, T. H. Lee, L. M. Leung, *J. Organomet. Chem.* **2006**, *691*, 4028–4041.
- [11] a) A. Morsali, M. Y. Masoomi, *Coord. Chem. Rev.* **2009**, *253*, 1882–1905; b) G. Mahmoudi, V. Stilinović, M. S. Gargari, A. Bauzá, G. Zaragoza, W. Kaminsky, V. Lynch, D. Choquesillo-Lazarte, K. Sivakumar, A. A. Khandari, A. Frontera, *CrystEngComm* **2015**, *17*, 3493–3502.
- [12] M. F. Nejad, M. R. T. B. Olyai, H. R. Khavasi, *Z. Kristallogr. New Cryst. Struct.* **2010**, *225*, 717–718.
- [13] a) P. Baran, R. Boca, M. Breza, H. Elias, H. Fuess, V. Jorik, R. Klement, I. Svoboda, *Polyhedron* **2002**, *21*, 1561–1571; b) X. Gong, Y. Y. Ge, M. Fang, Z. G. Gu, S. R. Zheng, W. S. Li, S. J. Hu, S. B. Li, Y. P. Cai, *CrystEngComm* **2011**, *13*, 6911–6915.
- [14] M. Shakir, M. Azam, Y. Azim, S. Parveen, A. U. Khan, *Polyhedron* **2007**, *26*, 5513–5518.
- [15] J. Kumar, M. J. Sarma, P. Phukan, D. K. Das, *Dalton Trans.* **2015**, *44*, 4576–4581.
- [16] a) H. P. Zhou, X. P. Gan, X. L. Li, Z. D. Liu, W. Q. Geng, F. X. Zhou, W. Z. Ke, P. Wang, L. Kong, F. Y. Hao, J. Y. Wu, Y. P. Tian, *Cryst. Growth Des.* **2010**, *10*, 1767–1776; b) J. B. King, M. R. Haneline, M. Tsunoda, F. P. Gabbai, *J. Am. Chem. Soc.* **2002**, *124*, 9350–9351; c) E. Hupf, E. Lork, S. Mebs, J. Beckmann, *Inorg. Chem.* **2015**, *54*, 1847–1859.
- [17] a) A. W. Addison, T. N. Rao, J. Reedijk, J. Van Rijn, G. C. Verschoor, *J. Chem. Soc., Dalton Trans.* **1984**, 1349–1356; b) H. R. Khavasi, B. M. M. Sadegh, *Dalton Trans.* **2015**, *44*, 5488–5502.
- [18] a) B. Notash, N. Safari, H. R. Khavasi, *Inorg. Chem.* **2010**, *49*, 11415–11420; b) A. Sasmal, E. Garribba, C. Rizzoli, S. Mitra, *Inorg. Chem.* **2014**, *53*, 6665–6674.
- [19] Y. W. Dong, R. Q. Fan, P. Wang, L. G. Wei, X. M. Wang, S. Gao, H. J. Zhang, Y. L. Yang, Y. L. Wang, *Inorg. Chem.* **2015**, *54*, 7742–7752.
- [20] a) X. J. Hong, M. F. Wang, H. Y. Jia, W. X. Li, J. Li, Y. T. Liu, H. G. Jin, Y. P. Cai, *New J. Chem.* **2013**, *37*, 933–940; b) M. F. Wang, X. J. Hong, Q. G. Zhan, H. G. Jin, Y. T. Liu, Z. P. Zheng, S. H. Xu, Y. P. Cai, *Dalton Trans.* **2012**, *41*, 11898–11906.
- [21] a) J. L. Wang, B. Liu, B. S. Yang, *CrystEngComm* **2011**, *13*, 7086–7097; b) J. Y. Wu, H. Y. Hsu, C. C. Chan, Y. S. Wen, C. Tsai, K. L. Lu, *Cryst. Growth Des.* **2009**, *9*, 258–262.
- [22] T. S. Basu Baul, S. Kundu, S. Mitra, H. Höpfl, E. R. T. Tiekink, A. Linden, *Dalton Trans.* **2013**, *42*, 1905–1920.
- [23] a) H. R. Khavasi, A. A. Tahrani, *CrystEngComm* **2013**, *15*, 5799–5812; b) L. Yang, D. R. Powell, R. P. Houser, *Dalton Trans.* **2007**, 955–964.
- [24] a) D. Dey, G. Kaur, A. Ranjani, L. Gayathri, P. Chakraborty, J. Adhikary, J. Pasan, D. Dhanasekaran, A. R. Choudhury, M. A. Akbarsha, N. Kole, B. Biswas, *Eur. J. Inorg. Chem.* **2014**, 3350–3358; b) M. Maiti, D. Sadhukhan, S. Thakurta, S. Roy, G. Pilet, R. J. Butcher, A. Nonat, L. J. Charbonnière, S. Mitra, *Inorg. Chem.* **2012**, *51*, 12176–12187; c) D. Sadhukhan, M. Maiti, G. Pilet, A. Bauzá, A. Frontera, S. Mitra, *Eur. J. Inorg. Chem.* **2015**, 1958–1972; d) J. G. Sole, L. E. Bausa, D. Jaque, *An Introduction to the Optical Spectroscopy of Inorganic Solids*, Wiley, Chichester, UK, **2005**.
- [25] a) C. Seward, J. Chan, D. Song, S. N. Wang, *Inorg. Chem.* **2003**, *42*, 1112–1120; b) E. V. Antina, R. T. Kuznetsova, L. A. Antina, G. B. Guseva, N. A. Dudina, A. I. V'yugin, A. V. Solomonov, *Dyes Pigm.* **2015**, *113*, 664–674.
- [26] a) X. L. Yang, M. H. Xie, C. Zou, C. D. Wu, *CrystEngComm* **2011**, *13*, 6422–6430; b) J. J. Shen, M. X. Li, Z. X. Wang, C. Y. Duan, S. R. Zhu, X. He, *Cryst. Growth Des.* **2014**, *14*, 2818–2830; c) M. D. Allendorf, C. A. Bauer, R. K. Bhakta, R. J. T. Houk, *Chem. Soc. Rev.* **2009**, *38*, 1330–1352; d) S. Majumder, L. Mandal, S. Mohanta, *Inorg. Chem.* **2012**, *51*, 8739–8479.
- [27] Y. H. Wu, L. Chen, J. Yu, S. L. Tong, Y. Yan, *Dyes Pigm.* **2013**, *97*, 423–428.
- [28] F. Jin, H. Z. Wang, Y. Zhang, Y. Wang, J. Zhang, L. Kong, F. Y. Hao, J. X. Yang, J. Y. Wu, Y. P. Tian, H. P. Zhou, *CrystEngComm* **2013**, *15*, 3687–3695.
- [29] K. C. Stylianou, R. Heck, S. Y. Chong, J. Bacsa, J. T. A. Jones, Y. Z. Khimiyak, D. Bradshaw, M. J. Rosseinsky, *J. Am. Chem. Soc.* **2010**, *132*, 4119–4130.
- [30] a) O. Bolton, K. Lee, H. J. Kim, K. Y. Lin, J. Kim, *Nat. Chem.* **2011**, *3*, 205–210; b) H. Saigusa, T. Azumi, *J. Chem. Phys.* **1979**, *71*, 1408–1413; c) K. Hamanoue, T. Nakayama, I. Tsujimoto, S. Miki, K. Ushida, *J. Phys. Chem.* **1995**, *99*, 5802–5808.
- [31] a) Y. Hu, I. Sanchez-Molina, S. A. Haque, N. Robertson, *Eur. J. Inorg. Chem.* **2015**, 5864–5873; b) X. Y. Wang, A. D. Guerso, S. Baitalik, G. Simon, G. B. Shaw, L. X. Chen, R. Schmeh, *Photosynth. Res.* **2006**, *87*, 83–103.
- [32] a) F. Tancini, F. Monti, K. Howes, A. Belbakra, A. Listorti, W. B. Schweizer, P. Reutenauer, J. L. Alonso-Gómez, C. Chiorboli, L. M. Urner, J. P. Gisselbrecht, C. Boudon, N. Armaroli, F. Diederich, *Chem. Eur. J.* **2014**, *20*, 202–216; b) R. Tripiet, C. Platas-Iglesias, A. Boos, J. F. Morfin, L. Charbonnière, *Eur. J. Inorg. Chem.* **2010**, 2735–2745; c) P. Nikolov, I. Petkova, G. Köhler, S. Stojanov, *J. Mol. Struct.* **1998**, *448*, 247–254.
- [33] X. M. Wang, P. Wang, R. Q. Fan, M. Y. Xu, L. S. Qiang, L. G. Wei, Y. L. Yang, Y. L. Wang, *Dalton Trans.* **2015**, *44*, 5179–5190.
- [34] a) Y. N. Hong, J. W. Y. Lam, B. Z. Tang, *Chem. Commun.* **2009**, 4332–4353; b) M. Shellaiah, Y. H. Wu, A. Singh, M. V. R. Raju, H. C. Lin, *J. Mater. Chem. A* **2013**, *1*, 1310–1318; c) X. D. Yang, X. L. Chen, X. D. Lu, C. G. Yan, Y. K. Xu, X. D. Hang, J. Q. Qu, R. Y. Liu, *J. Mater. Chem. C* **2016**, *4*, 383–390.
- [35] a) T. L. Zhou, F. Li, Y. Fan, W. F. Song, X. Y. Mu, H. Y. Zhang, Y. Wang, *Chem. Commun.* **2009**, 3199–3201; b) F. Würthner, T. E. Kaiser, C. R. Saha-Möllner, *Angew. Chem. Int. Ed.* **2011**, *50*, 3376–3410; *Angew. Chem.* **2011**, *123*, 3436–3473; c) W. Y. Wong, L. Liu, J. X. Shi, *Angew. Chem. Int. Ed.* **2003**, *42*, 4064–4068; *Angew. Chem.* **2003**, *115*, 4198–4202.
- [36] a) Y. N. Hong, L. M. Meng, S. J. Chen, C. W. T. Leung, L. T. Da, M. Faisal, D. A. Silva, J. Z. Liu, J. W. Y. Lam, X. H. Huang, B. Z. Tang, *J. Am. Chem. Soc.* **2012**, *134*, 1680–1689; b) M. M. Cai, Z. Q. Gao, X. H. Zhou, X. P. Wang, S. F. Chen, Y. Z. Zhao, Y. Qian, N. Shi, B. X. Mi, L. H. Xie, W. Huang, *Phys. Chem. Chem. Phys.* **2012**, *14*, 5289–5296.
- [37] Y. W. Dong, R. Q. Fan, P. Wang, L. G. Wei, X. M. Wang, H. J. Zhang, S. Gao, Y. L. Yang, Y. L. Wang, *Dalton Trans.* **2015**, *44*, 5306–5322.
- [38] a) R. Z. Lakowicz, *Principles of Fluorescence Spectroscopy*, 2nd ed., Kluwer Academic/Plenum Publisher, New York, **1999**; b) H. Liu, T. Ye, C. Mao, *Angew. Chem. Int. Ed.* **2007**, *46*, 6473–6475; *Angew. Chem.* **2007**, *119*, 6593–6595; c) S. Chen, Y. K. Wu, Y. Zhao, D. N. Fang, *RSC Adv.* **2015**, *5*, 72009–72018.
- [39] G. M. Sheldrick, *SHELXTL NT Crystal Structure Analysis Package*, version 5.10, Bruker AXS, Madison WI, **1999**.

Received: March 3, 2016

Published Online: July 4, 2016